Università
Ca'Foscari
Venezia

Master's Degree in Sustainable Chemistry and Technologies

Final Thesis

Synthesis and characterization of luminescent copper(I) complexes with benzotriazole- and indazole-based N-donor ligands

Supervisor
Dott. Marco Bortoluzzi

Graduand
Valentina Ferraro
Matricolation number 854235

Academic Year
2019 / 2020

Index *Page*

1. Introduction

1.1 Luminescence in *d*-block elements

Luminescent complexes of *d*-block elements can be roughly divided in two categories depending on where the emitted photon comes from. Emissions of metal centres such as manganese(II) [1] and chromium(III) [2] are originated from multielectronic wavefunctions deriving from 3*d* orbitals. This behaviour can be compared to that of lanthanide(III) complexes, where spin-orbit levels deriving from 4*f* orbitals are involved. All these compounds belong to a first category where the photon is released by the metal centre and the ligands are implicated only in the population mechanism of the emitting levels [3]. As regards manganese(II), the colour of the emission is also connected to the geometry of the complex: tetrahedral compounds are commonly bright green, whereas octahedral derivatives are orange-red. Luminescence lifetimes are also strongly dependent upon the coordination sphere, being the $^4T_1(^4G) \rightarrow {}^6A(^6S)$ transition parity-forbidden for octahedral species but not for tetrahedral compounds.

On the contrary, in lanthanide(III) derivatives the 4*f* are core-orbitals, so they do not participate in the formation of the bonds. This characteristic generates peculiar optical proprieties, such as low dependence of the absorption and emission frequencies upon the coordination sphere and absence of vibrational structure in the spectra. These features lead to sharp bands compared to the ones typical of the *d*-block elements and the chromatic purity has made lanthanide(III) complexes very interesting from a technologic point of view. Moreover, the *f-f* transitions are Laporte-forbidden so they are characterized by micro- or milliseconds-long emissions [4].

The second category is composed by all the luminescent complexes where the photon is emitted from excited states involving molecular orbitals of the ligands. Several coordination compounds with d^6, d^8 and d^{10} metal centres, such as Re(I), Ru(II), Os(II), Ir(III), Pt(II), Au(I) and Au(III) complexes, belong to this group [5]. Their luminescent proprieties are connected to charge transfer mechanisms that, for instance, can occur from a filled *d* orbital of the metal centre to the antibonding orbitals of the ligands. This process, depicted as a blue arrow in Figure 1, is called “metal to ligand charge transfer” or MLCT. However, the opposite mechanism, illustrated as green arrow in figure below, exists too: an electron can be transferred

from the ligand to the metal centre with a mechanism known as “ligand to metal charge transfer” or simply LMCT. More rarely, it is possible to observe the transfer between coordinated ligands (LLCT, ligand-to-ligand charge transfer) or ligand-to-metal-to-metal charge transfer (LMMCT) in multinuclear complexes with strong metal-metal interactions [6]. Anyhow the luminescence can be also ligand-centred (LC) when the participation of transition metal orbitals is negligible. The situations initially described, where the ligand orbitals are instead poorly involved, are called metal-centred (MC) transitions. The last two conditions are respectively pictured as a red and yellow arrow in the Figure 1 reported below.

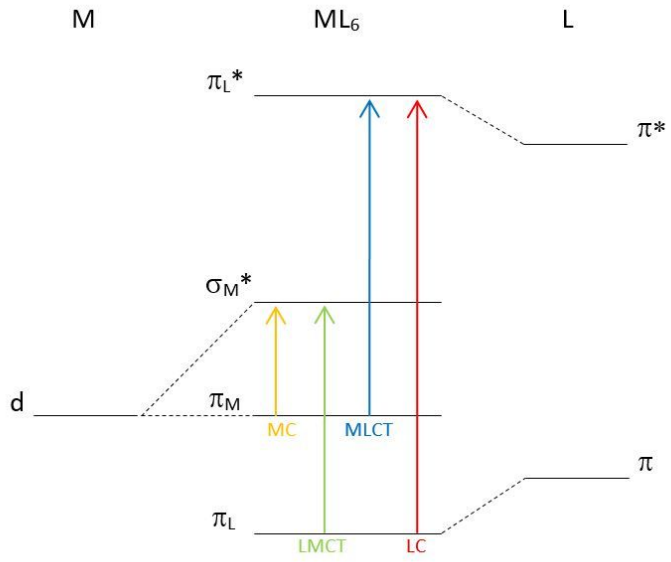

Figure 1. Molecular orbital diagram for a generic octahedral complex of a transition metal ML_6 and possible electronic transitions: MC (yellow arrow), LMCT (green arrow), MLCT (blue arrow) and LC (red arrow) mechanisms.

As regards photoluminescence, two main phenomena can be described: fluorescence (Figure 2a) and phosphorescence (Figure 2b). The former is a spontaneous emission that can be observed few nanoseconds after the exciting radiation is extinguished. It usually occurs at lower frequencies than the incident radiation because the emissive transition takes place after some vibrational energy has been discarded to the surroundings. Phosphorescence is a spontaneous emission as well, but it lasts for longer periods, typically from microseconds up to seconds. This difference is mainly attributable to the fact that only transitions having

the same multiplicity, as in the first case, are allowed (e.g. singlet → singlet); whereas phosphorescence is formally forbidden because it involves states of different multiplicity (e.g. triplet → singlet). This selection rule strongly limits the direct population by absorption of excited states with different multiplicity with respect to the ground-state. These excited states can be populated when the spin-orbit coupling is large, and consequently when the molecule contains a moderately heavy atom. In fact, if triplet and singlet excited states have a common geometry where their potential energy curves intersect, a molecule can undergo a non-radiative process called “intersystem crossing”, turning into a triplet-state [7].

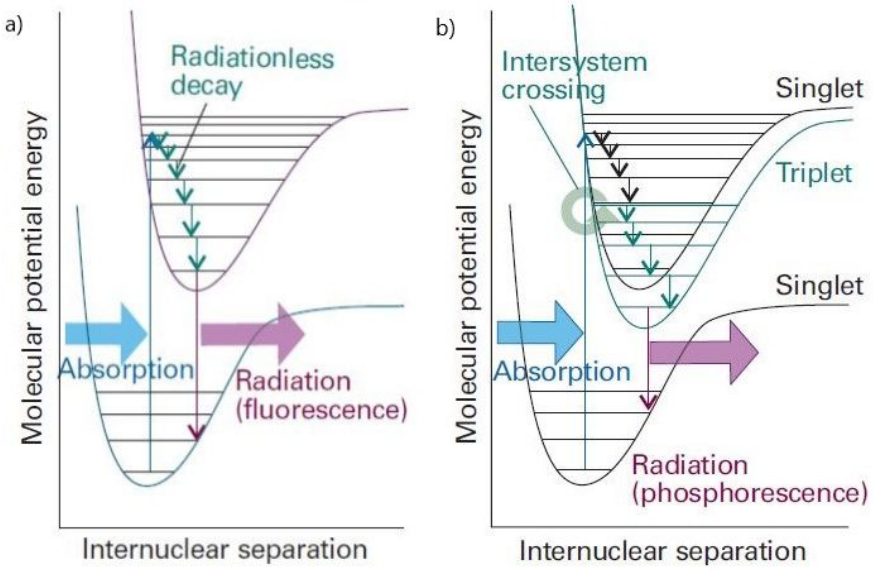

Figure 2. Comparison between the mechanisms leading to fluorescence (left) and phosphorescence (right).

The first luminescent complexes studied are based on d^6 metal ions of the second and third transition series, for example Ru(II) and Os(II). Aromatic bi- or tridentate heterocycles, such as 2,2’-bipyridine (bpy), have shown to be the most suitable ligands for these elements. One outstanding example is $[Ru(bpy)_3]^{2+}$, that combines high chemical stability under many conditions, excited-state reactivity, well defined redox proprieties, intense luminescent emission and microseconds-long excited-state lifetimes even in solution [8]. Another d^6 metal ion is Ir(III), which can coordinate bidentate cyclometallating ligands, for instance the deprotonated form of 2-phenylpyridine (Hppy), to afford the corresponding luminescent complexes. Even Re(I) carbonyl complexes bearing N-donor chelating ligands have been widely

investigated for their strong luminescence. Famous examples are tricarbonyl bipyridine derivatives having general formula $[Re(CO)_3(N^N)X]^{n+}$, where N^N is a diimine. The compounds can be neutral or cationic depending on the nature of X. Selected square-planar d^8 metal ions complexes, such as Pt(II) and Au(III) bearing both aromatic polydentate heterocycles and strong σ-donor ligands, have shown some interesting emissive features as well. Ag(I) and Au(I) can also afford complexes whose luminescent proprieties are attributable to mixed MLCT/MC mechanisms. Selected examples of luminescent second- and third-row transition derivatives are depicted below in Figure 3 [5c*;* 6b].

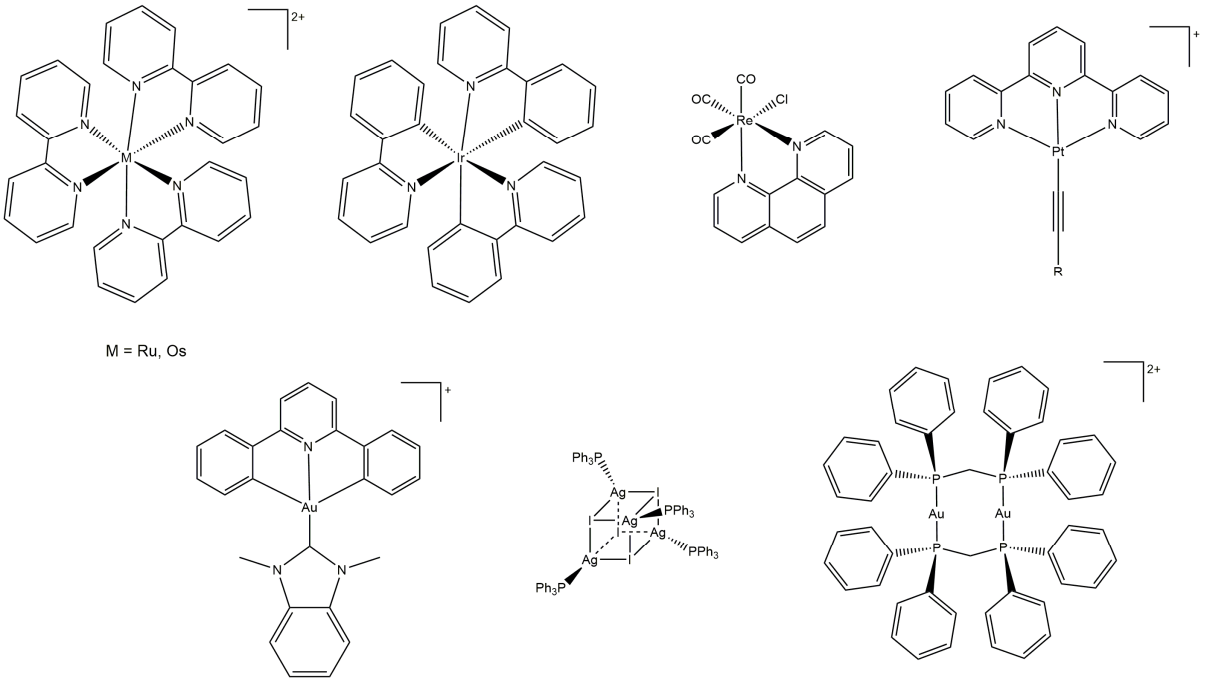

Figure 3. Examples of second and third transition metals luminescent complexes.

1.2 Luminescence in copper complexes

Nowadays most of the luminescent complexes applied in technology are based on lanthanides and *d*-block metals of the second and third transition series. For example, Pt(II) and Ir(III) complexes are commonly used as emitters for OLEDs (organic light emitting diodes) due to their long-lived triplet states [9]. However, recent studies have demonstrated that it is also possible to obtain highly luminescent complexes based on the first-row transition elements, such as Cr(III), Fe(III), Mn(II)

and Cu(I). Some examples are reported in Figure 4. The use of these metals has some advantages such as the lower expensiveness and toxicity, as well as their higher abundance [10].

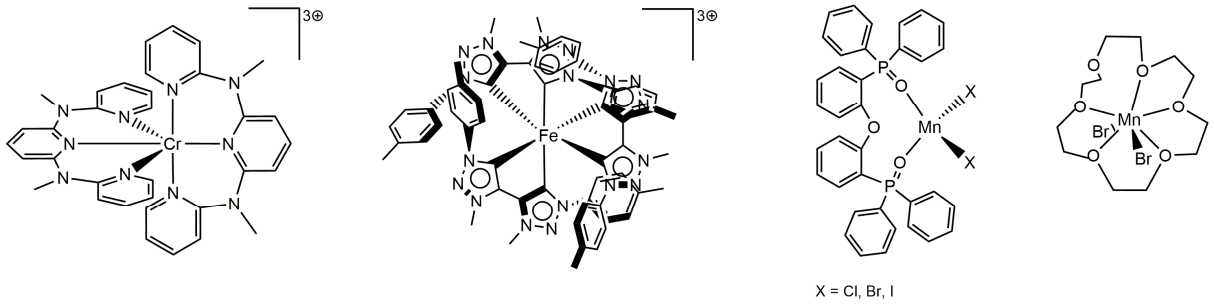

Figure 4. Examples of Cr(III), Fe(III) and Mn(II) luminescent complexes. From left to right: $Cr(ddpd)_2^{3+}$ (ddpd = N,N′-dimethyl-N,N′-dipyridine-2-ylpyridine-2,6-diamine), $Fe(btz)_3^{3+}$ (btz = 3,3-dimethyl-1,1-bis(*p*-tolyl)-4,4-bis(1,2,3-triazol-5-ylidene), Mn(DPEPO)X_2 [DPEPO = bis{2-(diphenylphosphino)phenyl}ether oxide], $MnBr_2$(18-crown-6).

As regards copper, this first-row transition element is characterized by an atomic number of 29 and it belongs to the same periodic table group of silver and gold. Its atomic configuration is $[Ar]3d^{10}4s^1$ and the two main oxidation states are 1+ (d^{10}) and 2+ (d^9). In aqueous solution and in absence of coordinating ligands, the reduction potentials are:

$Cu^{2+} + e^- \rightarrow Cu^+$ ($E^0 = 0.15$ V) $\qquad$ $Cu^+ + e^- \rightarrow Cu^0$ ($E^0 = 0.52$ V)

Therefore, $2\ Cu^+ \rightarrow Cu^{2+} + Cu^0$ is thermodynamically favourable ($E^0 = 0.37$ V) and the equilibrium constant is around 10^6, that implies that copper(I) is normally unstable in aqueous solution and tends to disproportionate. However, poorly soluble compounds such as CuCl, CuI and CuCN are resistant towards disproportion and, in general, the stability of Cu(I) can be increased in the presence of coordinating ligands. On the other hand, copper(I) is soluble in non-aqueous solvents, such as acetonitrile, where it affords the isolable complex $[Cu(NCCH_3)_4]^+$.

Cu(I) derivatives are normally characterized by coordination numbers of 2, 3 and 4. As regards the last one, the geometry is typically tetrahedral to minimize steric repulsions. Copper(II) can also have coordination number of 4 but, due to the Jahn-Teller effect, the geometry is distorted and can also be square planar. Cu(II) compounds can also have higher coordination numbers, 5 and 6 in particular.

As concerns copper(I), the electronic distribution is symmetric because of the completely filled d^{10} configuration that also prevents *d-d* metal centred electronic transitions. For this reason, the derivatives are normally diamagnetic and colourless, but they can have emitting proprieties associated with MLCT mechanism in the presence of suitable ligands. In fact, after the transition, the metal centre is formally oxidized to Cu(II) while the ligand is reduced, therefore π-conjugated systems are extremely important.

On the other hand, Cu(II) compounds are paramagnetic, owing to the presence of an unpaired electron. In this case *d-d* transitions are possible, so the derivatives are commonly characterized by absorptions in the visible or NIR region and they are usually blue-green coloured. However, because of the accessible non-radiative decay from the excited- to the fundamental-state, the complexes do not show luminescent proprieties.

The interest towards Cu(I) luminescent derivatives is mainly attributable to their peculiar emission features, whose lifetime and temperature dependency are deeply influenced by the ligands coordinated to the metal centre. Differently from lanthanides, changes in the ligands will alter the frontier molecular orbitals and therefore the emission colour. Colour tuning is one of the major driving forces of the recent studies concerning these complexes [11].

The earliest example of light-emitting copper complexes is $[Cu_4(\mu^3\text{-}I)_4(py)_4]$ (py = pyridine), containing the $\{Cu_4I_4\}$ cubane unit. By simply changing the coordinating heterocycle (e.g. with functionalized pyridines, picoline, quinoline or piperidine) other Cu_4I_4 clusters have been synthesised, all characterized by a large Stokes shift, *i.e.* a great energy difference between the band maxima in the absorption and emission spectra. Large Stokes shifts in cubane complexes are due to geometry distortions from the ground- to the excited-state, related to the interactions among the copper atoms in the Cu_4 cluster [12].

In the 80s, $[Cu(PPh_3)(phen)]^+$ (phen = 1,10-phenantroline) was investigated and it appeared to be the first metal-based TADF (thermally activated delayed fluorescence) material. This propriety is extremely interesting for optoelectronic applications and it was later applied in OLED technologies. When materials of this kind are excited, two separate mechanisms can be observed: the promoted (PF) and the delayed fluorescence (DF). The former corresponds to an immediate fast-decay

emission from the S_1 to the S_0 state. On the contrary, during the latter, triplet excitons have to be converted into singlets through a mechanism called “reversed intersystem crossing” (RISC). For this reason, the luminescent process seems to be delayed and consequently the fluorescent lifetimes are increased up to microseconds. To enhance the luminescent proprieties, the RISC ($T_1 \rightarrow S_1$) has to be efficient in order to harvest the triplet excitons. A small energy difference at room temperature between the singlet ^{1}MLCT and the triplet ^{3}MLCT excited states is the key feature of the process. This condition is observable in the blue-emitting complexes Cu(DPEPhos)(pz_2BPh_2), where DPEPhos is {bis[2-(diphenylphosphino)phenyl]ether} and pz_2BPh_2 is bis(pyrazol-1-yl)-biphenyl-borate, and [Cu(μ-I){Ph_2P-(o-C_6H_4)-$N(CH_3)_2$}$_2$]$_2$ (*cfr.* Figure 5). To achieve an efficient RISC, it is necessary to reduce the exchange interaction between HOMO (Highest Occupied Molecular Orbital) and LUMO (Lowest Unoccupied Molecular Orbital), in other words they have to be spatially separated. In this way excited singlet and triplet states will have comparable energies. Finally, the rate constant of the RISC process must be higher than that of phosphorescent decay to achieve TADF luminescence [13].

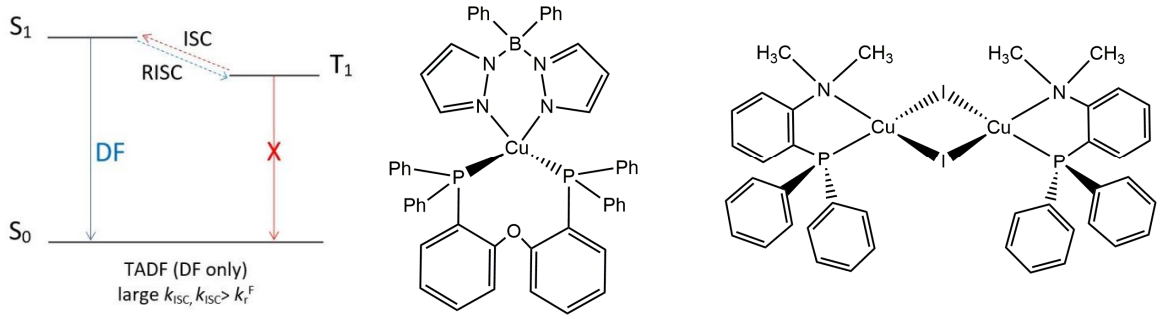

Figure 5. TADF mechanism and exemplifying Cu(I) complexes where it can be observed.

Nevertheless, systematic studies concerning luminescent copper complexes date back to the 90s due to the difficult harvesting of the $T_1 \rightarrow S_0$ transition, associated to long phosphorescence decay. Another complication is related to the non-emissive decay due to the Jahn-Teller flattening distortion after the MLCT excitation and the instability of the complexes in the excited-state. As shown in Figure 6, the different geometries of ground- (tetrahedral) and excited- (distorted tetrahedral or square planar) states can favour non-radiative decay processes with consequent reduction of quantum yield Φ. For this reason, the bulk of the ligands plays a role of paramount

importance in the luminescence of Cu(I) derivatives. Moreover, because of the formal change in the oxidation state the metal can coordinate a new ligand, namely solvent molecules or counterions, to fulfil an available site in the perpendicular position of the Cu(II) square planar excited species, originating a penta-coordinated excited complex, known as “exciplex”, that can follow non-radiative decay routes [11].

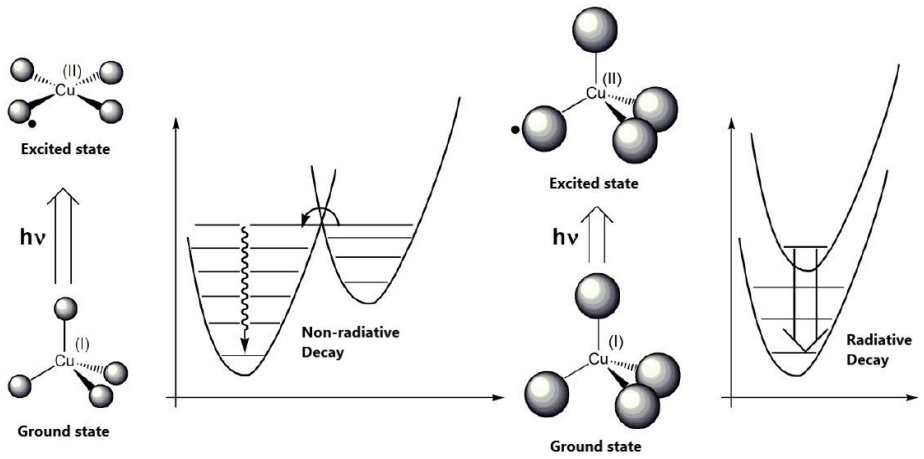

Figure 6. Non-radiative and radiative decay paths in tetrahedral Cu(I) complexes.

Unlike d^6 metal ion complexes, especially ruthenium(II) ones, that can be strongly affected by the presence of energetically close MC levels causing non-radiative deactivation pathways and photochemical degradation, copper(I) derivatives do not suffer from these kinds of problems. Despite that, vibrational modes and distortions of the coordination sphere in the excited-state can determine non-radiative deactivation processes. For this reason, emissions are generally weak in solution, even in the absence of O_2. Non-radiative pathways can also be favoured by other factors: for example, oxidative quenching can occur with nitroaromatic compounds, Co(III) and Cr(III) complexes and bipyridium salt derivatives. Quenching can also be observed as a consequence of energy transfer to molecules with low triplet states like anthracene [14].

Copper(I) complexes can be mainly divided, depending on their charge, into anionic, neutral and cationic compounds. Unlike the others, the first ones do not show particular photophysical proprieties, such as luminescence. On the other hand, neutral ad cationic complexes bearing chelating N- and P-donor ligands have been widely investigated. Normally, 1,10-phenantroline is used as chelating imine ligand to afford homoleptic and heteroleptic motifs such as $[Cu(N\hat{}N)_2]^+$ and $[Cu(N\hat{}N)(P\hat{}P)]^+$.

However, $[Cu(phen)_2]^+$ is non-emissive at room temperature and has an excited-state lifetime lower than 10 ns. On the contrary, the presence of alkyl and aryl groups in the 2,9-positions affords complexes characterized by a long-lived triplet-state. This difference is attributable both to the stabilization of the tetrahedral geometry and the increased energy gap between MLCT and ground-states. Probably the most representative of these complexes is $[Cu(dmp)_2]^+$ (dmp = 2,9-dimethyl-1,10-phenantroline, also known as “neocuproine”) that exhibits a broad unstructured emission at λ_{max} = 730 nm and a 85-ns-long excited-state. The schematic emission processes of this complex are depicted below (see Figure 7).

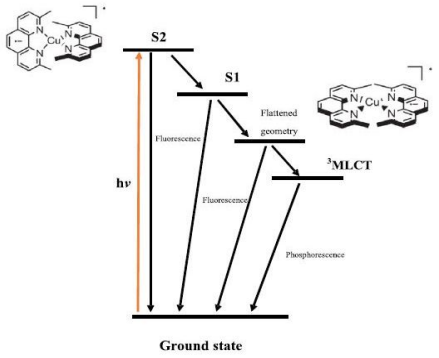

Figure 7. Schematic emission processes of $[Cu(dmp)_2]^+$ [11].

The luminescence of this species is however quenched by the presence of Lewis bases or coordinating solvents. On the basis of the results achieved using dmp as ligand, a huge number of 2,9-disubstituted phenanthroline ligands has been investigated, some of them sketched in Figure 8. [15]

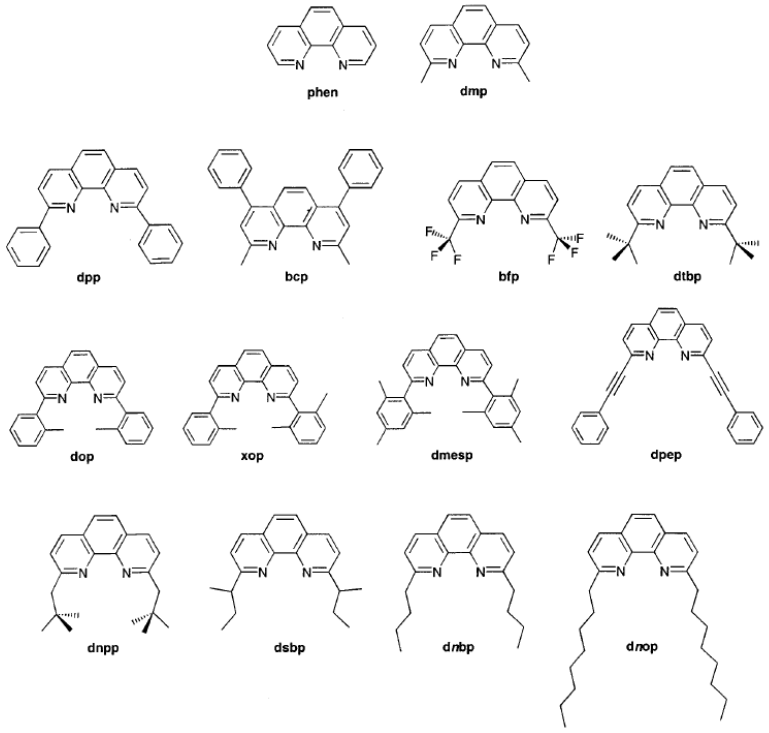

Figure 8. 1,10-phenantroline derivatives and their abbreviations.

Heteroleptic complexes, such as $[Cu(N\text{^}N)(PPh_3)_2]^+$ (N^N = 2,2'-bipyridine, 1,10-phenantroline and 2,9-dimethyl-1,10-phenantroline), have been widely investigated due to their high luminescence in solid-state and long excited-state lifetimes. In N-P mixed complexes, DFT (Density Functional Theory) calculations have demonstrated that the HOMO normally involves the lone pairs of the P^P ligand and Cu(I) *d* orbitals, while the LUMO is mainly constituted by the antibonding overlap of the N^N *p* orbitals. The use of a chelating phosphine like DPEPhos affords compounds characterized by superior emission proprieties, probably because of the higher stability of the coordination sphere associated to the chelating effect. Moreover, in these kinds of systems the charge transfer is improved by the presence of a wide P-Cu-P angle, causing also the enhancement of the emission lifetimes at room temperature. Examples of homoleptic and heteroleptic complexes bearing dmp as ligand are depicted in Figure 9 [16].

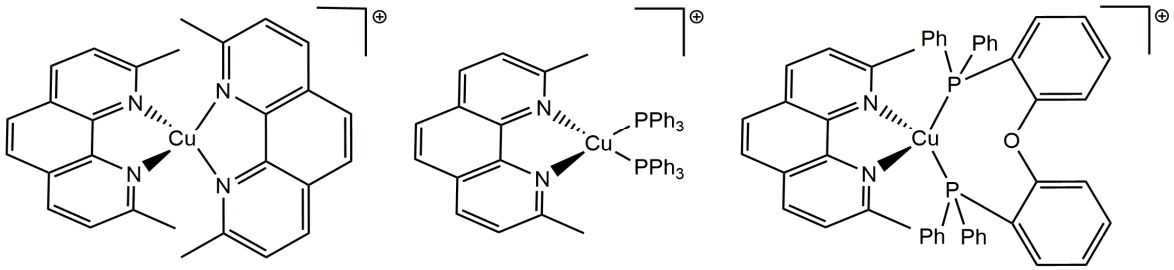

Figure 9. $[Cu(dmp)_2]^+$, $[Cu(dmp)(PPh_3)_2]^+$ and $[Cu(dmp)(DPEPhos)]^+$.

Another example of the role of the ligands in the luminescence of Cu(I) complexes is given by the use of N-[1-(2H-indazol-2-yl)ethylidene]-2,6-diisopropylaniline (N^N) as ligand. The comparison between $[Cu(N^N)_2]^+$ and $[Cu(N^N)(P^P)]^+$ [P^P = DPEPhos, dppe, PPh_3; dppe = 1,2-bis(diphenylphosphino)ethane] complexes, sketched in Figure 10, displays that the emission in glassy matrix of the former is blue-shifted and much shorter ($\tau \approx$ 280 ps) compared to the other compounds. The overall luminescence of the N-P mixed complexes is instead similar, but also in this case the species bearing DPEPhos as P-donor ligand has shown the best structural and photophysical proprieties, revealing to be the most suitable for solid-state lighting (SSL) applications. The μs-long lifetimes indicate both a mixed ^{3}MLCT/^{3}LC mechanism and a strong involvement of the LC triplet-state. [17].

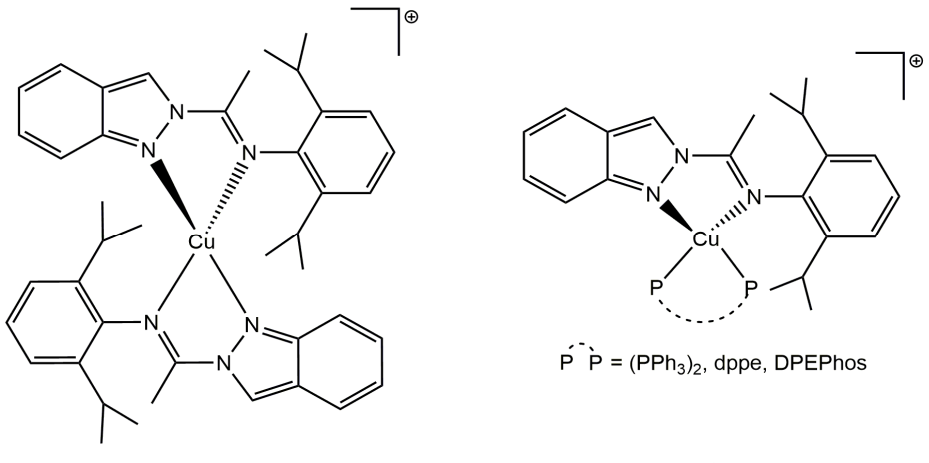

Figure 10. Homoleptic and heteroleptic Cu(I) complexes having N-[1-(2H-indazol-2-yl)ethylidene]-2,6-diisopropylaniline as ligand.

As regards the possibility of tuning the emission colour, the introduction of alkyl groups in the N^N ligand causes the hypsochromic (blue) shift of the absorption maxima. For instance, the bands move to shorter wavelengths by introducing in 2,9-

positions of the 1,10-phenantoline skeleton the methyl (dmp) and *n*-butyl (dnbp) fragments [18].

On the other hand, the extension of the π-conjugation achievable with the introduction of phenyl groups causes the shift of the spectral maxima to longer wavelengths, the so-called bathochromic or red shift. As an example, N-P mixed complexes bearing PPh_3 or DPEPhos have been investigated with biquinoline (bq) derivatives as N-donor ligands. The coordination of species such as dpbq (4,4'-diphenyl-2,2'-biquinoline) and mdpbp (3,3'-methyl-4,4'-di-phenyl-2,2'-biquinoline) allowed to obtain orange- and red-emitting complexes, whose luminescent features appeared to be enhanced probably because the rigid structure reduces the structural reorganization upon photoexcitation [19].

Another significant aspect of Cu(I) complexes, besides the long-lasting luminescence and the large Stokes shifts, is the possibility of influencing the emission proprieties with external stimuli, such as temperature. The previously reported Cu_4I_4 clusters, e.g. $[Cu_4(\mu^3\text{-}I)_4(py)_4]$ (see Figure 11a) have shown thermochromic proprieties, being their emission spectra characterized by two bands, one at high energy (HE) and the other at low energy (LE), as shown in Figure 11b. The two emissions are related to excited states of similar energies but involving different orbitals. Regardless the nature of the ligand, at room temperature the emission is dominated by the LE band, ascribable to a combination of a halide-to-metal-charge transfer (^{3}XMCT) and a cluster-centred (^{3}CC) transition. On the contrary, at low temperature this band is quite weak, and the luminescence is caused by a halide-to-ligand-charge transfer (^{3}XLCT) (see Figure 11c). As the antibonding orbitals of the ligand are involved, this band can be investigated only if unsaturated systems are present. Moreover, on lowering the temperature the LE band appears to be red-shifted, probably because of the stabilization of the ^{3}CC excited-state [20].

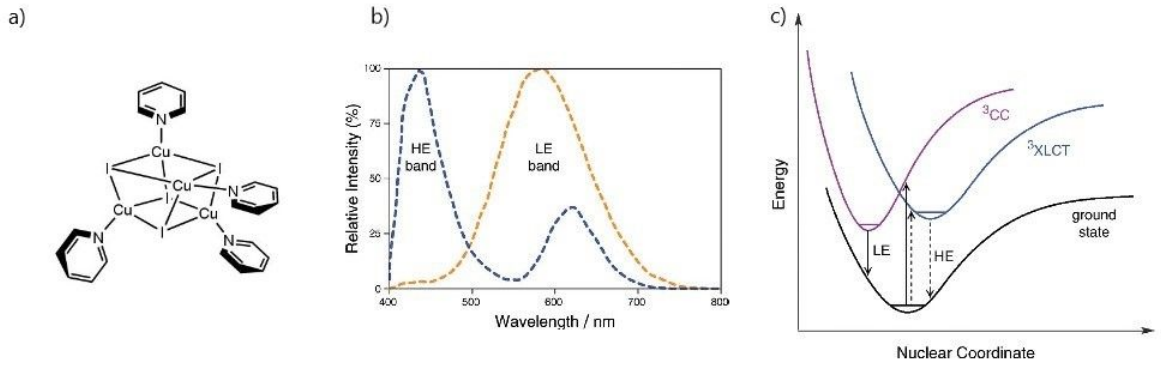

Figure 11. a) $[Cu_4(\mu^3\text{-}I)_4(py)_4]$ cluster; b) Normalized emission spectra of the $[Cu_4(\mu^3\text{-}I)_4(py)_4]$ cluster: the blue line is referred to the emission at -196 °C, while the orange one is at 25 °C; c) Simplified potential energy surface of the $[Cu_4(\mu^3\text{-}I)_4(py)_4]$ cluster.

Other common ways in which the luminescence can be triggered are vapochromism and mechanochromism. The former is particularly useful to detect VOCs (volatile organic compounds) and the changes in the luminescence features are attributable to reversible rearrangements catalysed by solvent vapour or interstitial solvation of transition metal coordination compounds. Interactions among the copper ions, π-π stacking and hydrogen bonding can be also influenced by the presence of interstitial solvent molecules. VOC molecules can also react with the complexes with the formation of metal-solvent bonds. All these aspects modify the energy of the excited state and therefore the emission. On the other hand, mechanochromism is the reversible change in the emission wavelength as a consequence of external mechanical forces like grinding, rubbing, shearing or compressing. Although this aspect has been investigated mainly for Au(I) and Pt(II), few examples concerning Cu(I) complexes bearing six-membered N-donor ligands have been reported. Mechanically-triggered luminescence is attributable to the disruption of internuclear Cu-Cu contacts, π-π stacking or changes in the molecular conformation. Thermal treatment or recrystallization can be used to return to the original emission. Mechanochromic complexes can be applied in various fields, such as mechanosensors and indicators, or optoelectronic devices [21].

Copper-based luminescent complexes can be obtained also with five-membered N-donor ligands, such as imidazole (Him). $[CuBr(PPh_3)_2Him]$ (see Figure 12a) has been synthesized and its luminescent proprieties have been fully investigated and rationalized on the basis of time-dependent DFT (TD-DFT) calculations. In this case,

the Cu-Br σ-bond plays a role of paramount importance in the emissive proprieties of the complex, being where the HOMO is mostly localized. As observable in Figure 12b and 12c, pyrazole heterocycles can also be included in polydentate N-donor ligands containing pyridine units. The complexes $[Cu(PPh_3)X]_2(\mu\text{-N^N})$, where X is I or Br and N^N is 3,5-bis[6-(2,2-dipyridyl)]pyrazole, are characterized by emissive proprieties in solid-state at room temperature attributable to interligand charge transfer (ILCT) and MLCT transitions. However, the formal substitution of Br with I implicates a bathochromic shift in the emission peak due to a weaker electron-donating effect of the former in contrast to the latter. Other examples of Cu(I) complexes with pyrazole-based ligands are compounds of general formula $[\{Cu_2(N^N)\}_2(\mu\text{-dppb})_2]^{2+}$, where N^N = 3-(2'-pyridyl)pyrazole, 5-tert-butyl-3-(2'-pyridyl)pyrazole or 5-trifluoromethyl-3-(2'-pyridyl)pyrazole and dppb = 1,4-bis(diphenylphosphino)butane. The comparison of these species shows an enhancement of the luminescent proprieties as a consequence of the substitution of the H or ^{t}Bu in the 5-position of the pyrazole ring with an electron-withdrawing CF_3 group [22].

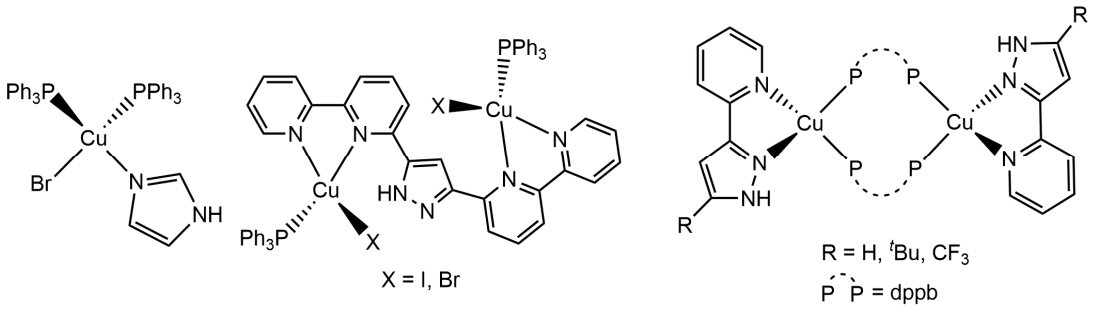

Figure 12. a) $[CuBr(PPh_3)_2Him]$; b) $[Cu(PPh_3)X]_2(\mu\text{-N^N})$ [X = I, Br; N^N = 3,5-bis{6-(2,2-dipyridyl)}pyrazole]; c) $[\{Cu_2(N^N)\}_2(\mu\text{-dppb})_2]^{2+}$ [N^N = 3-(2'-pyridyl)pyrazole, 5-tert-butyl-3-(2'-pyridyl)pyrazole, 5-trifluoromethyl-3-(2'-pyridyl)pyrazole; dppb = 1,4-bis(diphenylphosphino)butane].

Benzimidazole, triazole and tetrazole heterocycles can be used as N-donor ligands to afford luminescent Cu(I) compounds as well. Pyridine-heterocycles such as pyridine-benzimidazole (PyrBimH), -triazole (PyrTriH), -tetrazole (PyrTetH) and their conjugated bases have been systematically investigated in combination with phosphine moieties, such as PPh_3, dppm [1,1-bis(diphenylphosphino)methane] and DPEPhos. The neutral N^N ligands originate mononuclear cationic complexes both with PPh_3 and DPEPhos, that exhibit blue to green emissions ascribable to MLCT transitions. On the other hand, with the corresponding deprotonated ligand neutral

mononuclear motifs are achievable only with DPEPhos as P-donor ligand. In neutral complexes the luminescent proprieties are enhanced by the presence of tetrazole derivatives rather than benzimidazole- or triazole-based ligands. Selected examples of heteroleptic complexes are depicted in Figure 13 [23].

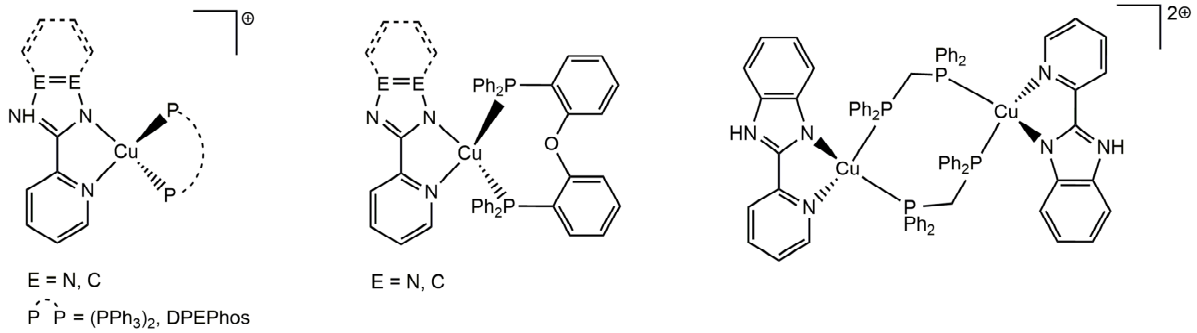

Figure 13. Examples of copper(I) complexes with five-membered N-donor ligands.

1.3 Copper coordination polymers

Another reason of interest concerning luminescent Cu(I) compounds is given by the fact that, in the presence of suitable ligands such as of halides, polynuclear species and coordination polymers characterized by unique electronic features are usually isolated. These solid-state materials are normally composed by connectors and linkers, respectively metal centres and halides or organic ligands. They are also known as MOFs or “metal-organic frameworks” if they possess a porous structure where a small molecule can be hosted. The structural rigidity of MOFs leads to unusual luminescent proprieties characterized by longer lifetimes and higher quantum efficiencies. MOFs can be widely used as sensors if they show a detectable and reversible change in response to a specific analyte, such as solvochromatic shift. Other proprieties that make luminescent MOFs suitable to be used as sensors are the alteration of the electronic structure by modification of the coordination sphere and the fluorescent quenching as a result of the absorption of species and the formation of exciplexes. An example is the Cu_6L_6 (L = 5,6-diphenyl-1,2,4-triazine-3-thiolate) cluster, that can be used to detect aromatic molecules (*i.e.* toluene, nitrobenzene, aniline, *o*-, *m*- and *p*-dimethylbenzene) in water. Cu(I) ions are coordinated to two sulphur and one nitrogen belonging to three different ligands. A bidimensional structure is obtained thanks to Van de Waals interactions among the

phenyl rings. As regards the detection of the analytes in water the distinct response of Cu_6L_6 to benzene-based species is attributable to π-π stacking interactions that, in the presence of monosubstituted benzene molecules and *o*-dimethylbenzene, can enlarge the Cu-Cu separation causing the efficient quenching of the luminescence. On the contrary, with *p*- and *m*-dimethylbenzene the aromatic-aromatic interactions in the cluster are only weakened, so the quenching is less effective [24].

Coordination polymers can be synthesized from copper(I) halides like CuCl, CuBr and CuI. The first two salts are air-unstable and they can be easily oxidized, so their dissolution in the presence of O_2 can lead to the formation of mixed-valence Cu(I/II) halide or Cu(II) halide complexes. CuX salts are poorly soluble in common organic solvents but they are moderately soluble in CH_3CN and CH_3CH_2CN. Ligands such as PPh_3 and similar phosphines can both stabilize the Cu(I) oxidation state and facilitate the solubilization of its salts.

Recently, hydro(solvo)thermal methods have also been applied for the synthesis of new copper(I) halide derivatives. In this case, the reactions are conducted in sealed Teflon reactors at 100-200 °C and under 10-30 atm of autogenous pressure. These conditions contribute to lower viscosity, facilitate the crystal growth and enhance the rate of solvent extraction, partially solving the solubility problems. As an example, this synthetic procedure has been used to obtain $\{[Cu_2(Htpim)(PPh_3)_2I_2]\cdot CH_3CN\}_n$ starting from CuI, PPh_3 and 2,4,5-tri(4-pyridyl)-imidazole (Htpim) in acetonitrile and methanol.

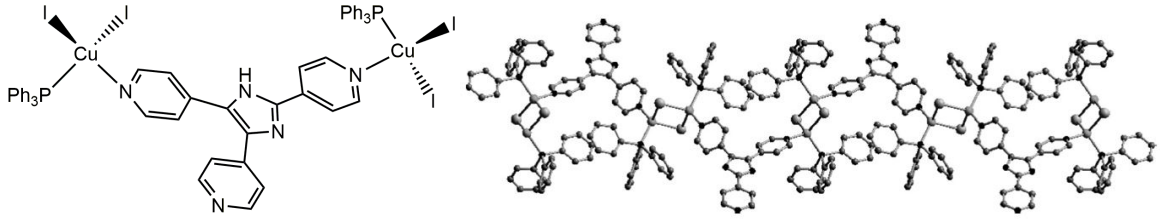

Figure 14. Copper(I) complex with Htpim and its zig-zag structure.

The complex reported in Figure 14 is characterized by a distorted tetrahedral structure where the Cu(I) coordinates a nitrogen atom of the pyridine moiety, a triphenylphosphine and two bridging I^- ions. The bridging mode of the anion leads to a CuI_2Cu rhomboid dimer, where PPh_3 and Htpim are in *trans* positions. The resulting zig-zag chained structure is obtained as the dimer is further connected to the

nitrogen atoms of the ligand. The coordination polymer shows a moderately intense red emission at 623 nm after being excited at 346 nm.

Oxidation and reduction routes can also be followed to afford the corresponding CuX (X = halide) aggregates respectively from Cu^0 and Cu(II). Coordination polymers based on copper(I) halides can have a large variety of possible structures, depending upon factors such as inner-core variability, outer-shell cooperativity and kinetic tunability. The first feature is connected to the fact that, as previously reported, copper(I) can have different coordination numbers and geometries, as well as the halide ions. Moreover, the organic ligands can influence the structure by acting as bridges among the Cu(I) centres. Then, the formation of CuX aggregates is controlled by kinetically fast associative/dissociative equilibria that can be tuned by changing the stoichiometric ratios of the reactants. As the crystallization process is normally slow, the isolated species may not be the most predominant in solution and their structure can hardly be predicted.

Depending on how many dimensions are involved, coordination polymers can be divided into zero-, one-, two- or three-dimensional ones. To the first category the previously reported Cu_4I_4 cubane derivatives can be included, whereas the $\{[Cu_2(Htpim)(PPh_3)_2I_2]\cdot CH_3CN\}_n$ species belongs to the second one. As regards two-dimensional motifs, $[Cu_3X(HT)_2]_n$ (X = Cl, Br, I; HT = 4-hydroxythiophenol) should be mentioned, especially because they show reversible thermochromic proprieties. The complexes deriving from CuCl and CuBr display strong orange emissions at room temperature, while the $[Cu_3I(HT)_2]_n$ aggregate is characterized by weaker luminescent proprieties. However, at 77 K the former ones strongly emit in the yellow region, while the latter in the green one upon excitation at 365 nm [25].

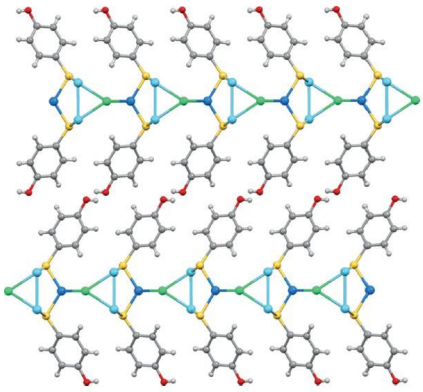

Figure 15: 2D structure of $[Cu_3I(HT)_2]_n$

$[Cu_4Br_4(bib)_2]_n$ [bib = 1,4-bis(imidazole-2-methyl)butane] is an example of 3D coordination polymer whose base unit consists of two independent Cu(I) ions, the same amount of bromides and neutral bib ligands [26].

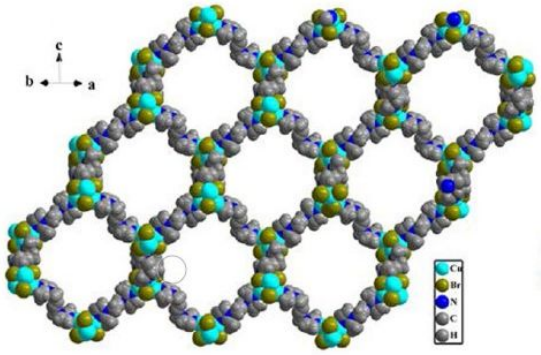

Figure 16. 3D framework of $[Cu_4Br_4(bib)_2]_n$

By varying the reaction conditions (solvent, temperature and template agents) it has been observed that it is possible to obtain coordination polymers having different dimensionality. For instance, different Cu(I) halide aggregates have been isolated using the triiimidazole ligand (L) depicted in Figure 17, which combines a unique photophysical behaviour and three nitrogen atoms available for coordination, increasing the number of possible structural motifs. The luminescent proprieties are attributable to concomitant fluorescence and ultralong phosphorescence connected to the formation $\pi-\pi$ stacking interactions in the crystal structure [27].

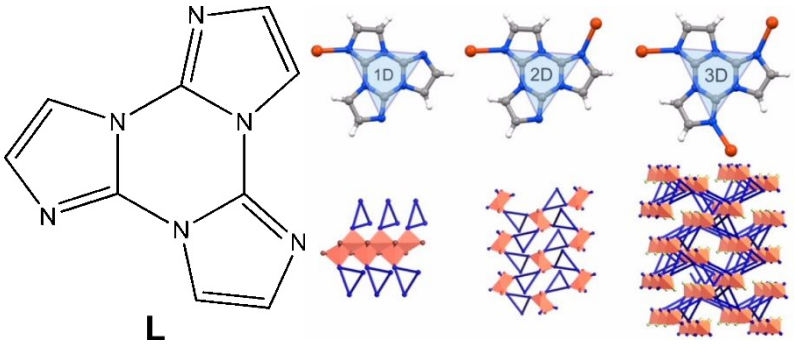

Figure 17. Triimidazole and corresponding 1D, 2D and 3D coordination polymers.

1.4 Applications

Copper(I) complexes have revealed to be suitable for solid-state lighting (SSL) applications, such as OLEDs and LECs.

As regards the formers, OLEDs are considered an interesting and greener alternative to the common LEDs since they are fabricated in less harsh conditions. Normally OLEDs are composed of anode, cathode, charge injection, light emissive and transport layers (see Figure 18). Holes and electrons are generated, and they move in opposite ways because of the Coulomb interaction, forming excitons in the emissive layers. Light is generated as a result of the energy transfer from the excitons to the emitting species.

OLED devices are typically fabricated by two possible processes: vacuum deposition or solution techniques (e.g. spin-coating, inkjet printing, casting, etc.). The former is the most common procedure and it works at high temperature and low pressure ($5 \cdot 10^{-5}$ mbar) to evaporate the layers on the ITO (indium tin oxide) substrate. The deposition over a large area is however difficult and the complexes need to be thermally stable. For this reason, this technique is usually applied to deposit volatile lanthanide complexes. On the contrary, solution processing methods are cheaper, less time consuming and they can be applied even in large areas under atmospheric conditions. These techniques are much more suitable for Cu(I) complexes because of their instability. Nevertheless, the film thickness is less controllable and the turn-on voltage (V_{ON}) is typically higher due to the presence of defects, like crystalline grains in functional layers. Since these imperfections behave like charge traps, they can provoke the emission quenching. The device performance is usually evaluated in terms of maximum electroluminescent quantum efficiency (EQE_{max}) and peak wavelength (λ_{max}), maximum current and power efficiency (CE_{max} and PE_{max}), turn-on voltage (V_{ON}) and maximum luminance (L_{max}).

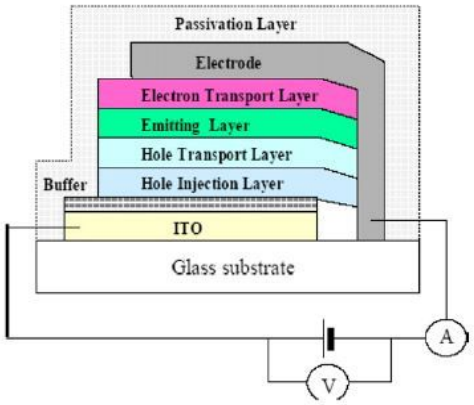

Figure 18: Multilayer OLED

Phosphorescent complexes based on elements of the third transition series, like Ir(III) and Pt(II), are commonly applied in OLED devices thanks to the extensive spin-orbit coupling that both facilitates the intersystem crossing and makes the spin-forbidden $T_1 \rightarrow S_0$ transition easy accessible. Even at room temperature the internal quantum efficiency is almost 100% when considering both singlet and triplet excitons. However, these metals are expensive and scarcely abundant, therefore there is a growing interest in copper derivatives. Some of the first examples of complexes applied in OLED devices are sketched in Figure 19. Anyhow, TADF has demonstrated to be a valid mechanism to harvest the triplet excitons. It is to be highlighted that, according to quantum mechanics, in statistical terms 25% of the excitons are singlets and the other 75% are triplets. In molecules characterized by thermally activated delayed fluorescence (TADF) the triplet excitons initially populating T_1 can be transferred to the S_1 level via RISC mechanism, while singlet ones at S_1 are radiatively deactivated to S_0 [28, 11, 13a].

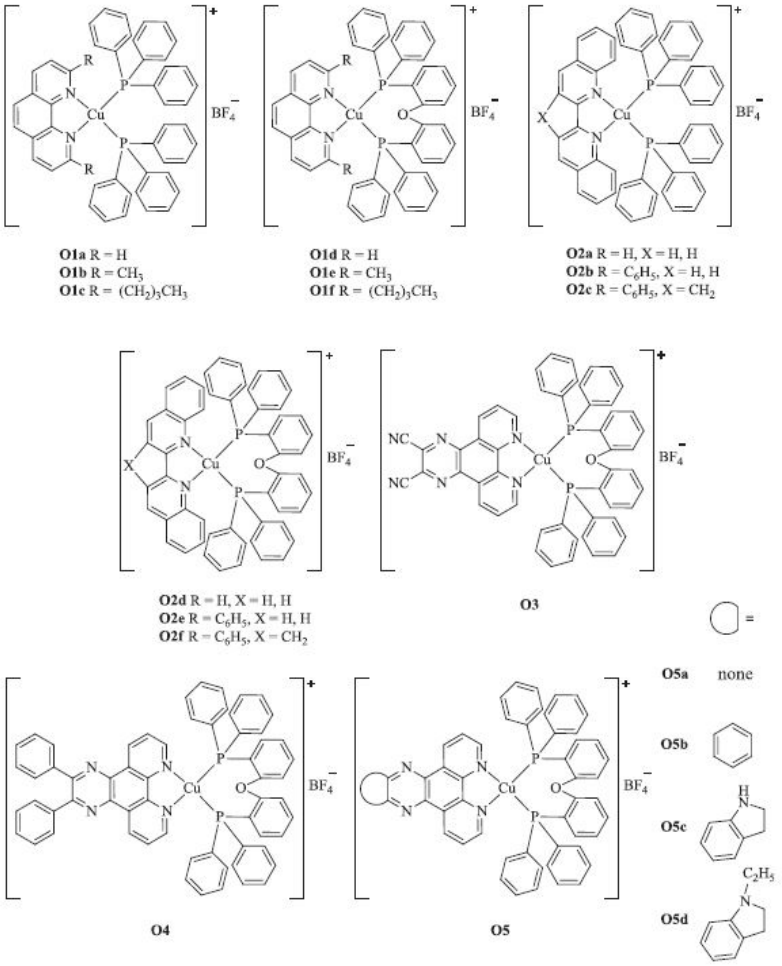

Figure 19. Examples of Cu(I) complexes applied in OLEDs technologies

Another possible application for luminescent copper(I) derivatives is given by LECs (light-emitting electrochemical cells), whose schematic structure is reported in Figure 20. These devices are simpler than OLEDs from a technological point of view. As they are processed from solution, they do not require air-sensitive charge-injection layers or metals for electron injection, and less strict packaging procedures are required. LEC devices are normally composed by two electrodes and between them an ionic luminescent material is inserted. The 100- or 200-nm-thick film can be a conjugated light-emitting polymer or an ionic transition metal complex (iTMC). In the first case, polymer-LECs or PLECs are originated; while in the second case they are called iTMC-LECs and, thanks to the ionic emitter, single-component devices can be afforded.

LECs work according to an unusual mechanism that can be explained through two theories: the electrodynamical (ED) and the electrochemical doping (ECD) models. As stated by both methods, upon the application of a potential, the separation of the

ions in the light-emitting layer narrows the injection barrier for electrons and holes. The former theory, shown in Figure 20a, presumes that electric double layers (EDLs) are formed at the electrodes thanks to the accumulation of ions. For this reason, near the electrode interfaces the electric potential drops and facilitates the injection from the electrodes. The light emission takes place in the bulk of the device, in the field-free region, where anions and cations are still united. On the contrary, according to the ECD model, depicted in Figure 20b, highly conductive *p*- and *n*- doped regions are assembled as a result of the accumulation of ions at the cathode and anode. *p*-doped or positive-doped regions are originated due to the removal of electrons; on the other hand, if they are added, *n*-doped or negative-doped regions are generated. These doped regions tend to broaden until a *p*-*i*-*n* junction (*i* = intrinsic, undoped) between them is originated. Across this area, the substantial drop of the applied voltage promotes charge recombination, thus light emission occurs.

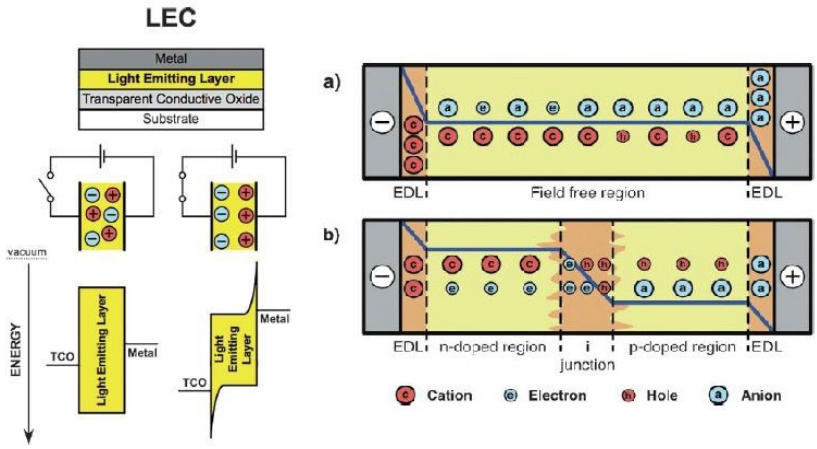

Figure 20. LECs schematic structure and mechanism of work.

Both theories have been confirmed by experimental data: the ED model is verified when in the organic film there is just a limited electron injection; whereas, when extensive electron injection takes place, doped zone are formed, as proposed by the EDC theory. Ionic motion determines both the speed of formation of the EDLs and the broadening of the doped zone. In iTMC-LECs the phosphorescence originating from the long-lived triplet excitons is responsible for the light emission but, as the *p*- and *n*-doped regions broaden at expense of the neutral layer, LEC luminance will inevitably quench over time. Chemical degradation and reduction in the thickness of the emitting layer are behind the declining of LEC luminance, but this process can be

inverted simply by turning the device off once the maximum luminance is achieved and re-applying the same potential.

The first PLECs were based on polymers such as poly[5-(2'-ethylhexyloxy)2-methoxy-1,4-phenylene vinylene] (MEH-PPV) and poly-(ethylene oxide) (PEO), and Li[CF_3SO_3] (see Figure 21). Instead, the earliest complex applied in LECs technology is the orange-emitting [Ru(vbpy)$_3$][PF_6]$_2$ (vbpy = 4-vinyl-4'-methyl-2,2'-bypiridine). Besides being the emitting species, the Ru(II)-derivative and its anion play a role of paramount importance since they promote charge injection, electron and hole transport through the device. The same tasks are nowadays covered by emitting ionic biscyclometalated Ir(III) complexes, as their emission can be tuned from blue to red whereas the luminescence of Ru(II)-derivatives is limited to the orange-red region.

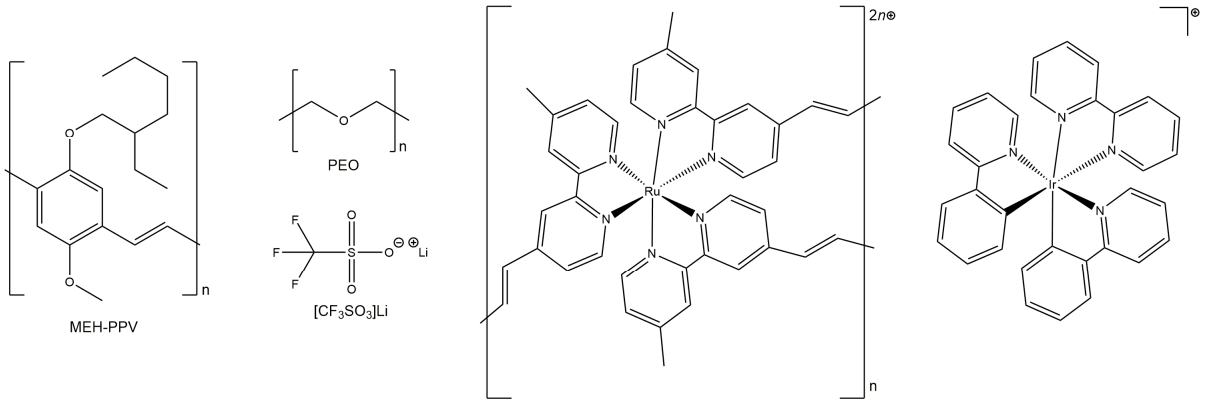

Figure 21. PLECs and iTM-LECs main constituents

LECs can be characterized according to their luminance (L), current density (J), turn-on time (t_{ON}), lifetime ($t_{1/2}$), total emitted energy (E_{TOT}), efficacy (or current efficiency), power efficiency and external quantum efficiency (EQE). $t_{1/2}$ and E_{TOT} are two markers of the stability of a LEC device, being the former the time needed to achieve half the luminance and the latter the integration of the radiant flux from t = 0 to t = $t_{1/5}$, where $t_{1/5}$ is the time to reach one fifth of the maximum luminance [29].

Copper(I)-based LECs have also been investigated thanks to their advantages with respect to derivatives of elements of the second and third transition series. An example is the dinuclear Cu(I) complex reported in Figure 22 that bears dmp and tetrakis[di(2-methoxyphenyl)-phosphanyl]cyclobutane (o-MeO-dppcb) as ligands. The compound was chosen as possible emitter for LEC devices thanks to its high quantum yield (Φ = 49 %) and 13.8-μs-long excited-state lifetime. Moreover, as its

TADF proprieties allow to collect both singlet and triplet excitons, it is the first case of singlet harvesting effect. The LEC device fabricated consists of ITO glass substrate, Al cathode and $[Cu(dmp)_2(o\text{-}MeO\text{-}dppcb)][PF_6]_2$ sandwiched between them after being embedded in a matrix of poly(3,4-ethylenedioxythiophene)polystyrene sulfonate [16d].

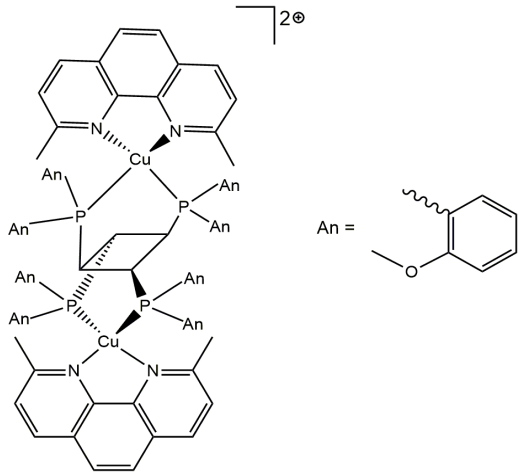

Figure 22: $[Cu(dmp)_2(o\text{-}MeO\text{-}dppcb)][PF_6]_2$

In LEC devices the presence of an electrolyte in the active layer promotes the injection of electrons and holes, thus the luminescence. However, light emission can also be induced by a luminophore formed thanks to an electron transfer reaction between the electrochemically active species. The so-obtained device is called ECLD, *i.e.* electrogenerated chemiluminescence or electrochemiluminescent device, and it has been widely applied in analytical techniques due to the extreme sensitivity to the electrochemical environment of the analyte solution. The electrochemiluminescence mechanisms can be divided into two categories: the annihilation and the coreactant ECL. The former implies that the electron transfer reaction occurs between the oxidized and the reduced species of the luminophore. The previously reported $[Ru(bpy)_3]^{2+}$ can emit light upon relaxation to the ground-state of the excited $[Ru(bpy)_3]^{2+*}$, that was obtained from the reaction between the reduced $[Ru(bpy)_3]^{+}$ and the oxidized $[Ru(bpy)_3]^{3+}$. On the other hand, the latter mechanism requires the presence of a coreactant to afford the excited-state of the luminophore, for example tripropylamine (TPrA) or oxalate ($C_2O_4^{2-}$). In this case, the excited $[Ru(bpy)_3]^{2+*}$ is obtained as a result of the reaction between $[Ru(bpy)_3]^{3+}$ and TPrA· or $CO_2^{\cdot-}$, that have been electrochemically generated from the coreactants.

This process is called “oxidative-reductive” coreactant ECL and, due to the high sensitivity towards the quantity of the coreactant, it is frequently used for analytical purposes.

Typical luminophores based on transition metals are Ru(II) and Ir(III) derivatives. However, Cu(I)-based ECLDs for the detection of copper ions in water have been investigated. The previously reported $[Cu(dmp)_2]^+$ has been generated from Cu ions, dmp and TPrA and, according to the intensity of the electrochemiluminescence, it was possible to determine the quantity in ppm of copper in the aqueous solutions considered. Besides the luminophore, an electrolyte is mandatory to form oxidized and reduced states. The mixture between luminophore, electrolyte and eventually coreactant originates a liquid solution that represents a drawback in electronic applications, where a solid-state device is usually preferred.

Although LECs and ECLDs may appear pretty similar, in reality they are completely different. First of all, the amount of luminophore is predominant with respect to the electrolyte in LECs (approx. 10:1), but not in ECLDs, where the typical ratio is approximately 1:10. In the former, the electrolyte promotes the injections of electrons and holes into a solid-state luminophore film though sequential hopping processes before recombination. Normally these devices operate in DC (direct current) bias, but few reports of AC-driven (alternate current) LECs can be found. Electrons and holes are carried by a conductive process, while in ECLDs the convective one is crucial as luminescence is reached when oxidized and reduced species meet in the electrolyte. In this case, a small amount of luminophore moves inside the liquid or gel electrolyte, and for this reason the device response is generally slow. This problem may be avoided by operating in AC. Increasing the concentration of the luminophore may lead to an enhancement of the light intensity, but this process is limited by the solubility inside the electrolytic solution [30].

Table 1: Comparison between ECLD and LEC characteristics

	ECLD		LEC	
active layer composition (wt %)	electrolyte (major)	[EMIM][TFSI] (10)	electrolyte (minor)	[EMIM][TFSI] (1)
	luminophore (minor)	$[Ru(bpy)_3][(PF_6)_2]$ (1)	luminophore (major)	$[Ru(bpy)_3][(PF_6)_2]$ (10)
delivery of electrons and holes	convective transport (luminophores are used as a shuttle)		conductive transport (sequential hopping occurs between neighboring luminophores)	
effective operation method	AC	500 Hz, ±3 V	DC	6 V
response time	short (<ms)	0.2–0.3 ms	long (>s)	1 min
max. intensity	weak	700 cd/m^2	strong	>4000 cd/m^2

1.5 Aim of the thesis

The aim of the thesis is the synthesis and characterization of new luminescent mononuclear and polynuclear copper(I) complexes based on mono- and polydentate benzotriazole and indazole derivatives, following the results previously reported [31]. The photophysical proprieties will be experimentally investigated and rationalized by DFT and TD-DFT calculations. After their emissive features are determined, the complexes will be applied in the preparation of doped plastics to be used in light sources. Technological applications such as the preparation of coatings for white LEDs will be explored.

2. Experimental part

2.1 Reagents and solvents

Copper(II) sulfate pentahydrate, copper(II) chloride and all the other reagents employed are from Aldrich, Carlo Erba or TCI and they were used without further purification. Anhydrous $CoCl_2$ was obtained from the corresponding hexahydrated salt using an Abderhalden's drying pistol heated in the presence of P_4O_{10} with refluxing toluene. The solvents employed for the reactions inside the glove box were dried according to literature procedures, whereas for the other syntheses the commercially available solvents were used without any treatment [32].

Both copper(I) bromide and chloride were prepared according to literature procedures using sodium sulphite as reducing agent [33]. To obtain copper(I) bromide, a solution containing 2.100 g of Na_2SO_3 in 3.50 mL of water is added dropwise at room temperature to a stirred solution of 5.293 g of $CuSO_4 \cdot 5H_2O$ (21.2 mmol) and 5.195 g of NaBr (50.5 mmol) in 30 mL of water. The resulting mixture is subsequently heated at 60 °C for 5 minutes and it is stirred at this temperature for 10 minutes. Then the solution is left cooling down to room temperature. After one hour the supernatant phase is eliminated and CuBr is collected as a white precipitated. The solid is washed twice with 10 mL of distilled water and stored inside the glove box.

On the other hand, copper(I) chloride was prepared starting from a solution containing 4.995 g of $CuCl_2 \cdot 2H_2O$ (29.3 mmol) in 5 mL of distilled water. A mixture of 3.800 g of Na_2SO_3 in 25 mL of distilled water is added dropwise to the previous solution under stirring and at room temperature. The mixture becomes first dark brown and then white CuCl slowly separates. The precipitate and the surnatant liquid are subsequently poured into a solution containing 500 mL of water, 0.500 g of Na_2SO_3 and 1 mL of concentrated HCl. Then the mixture is stirred and after sedimentation the surnatant liquid is decanted, while the solid is washed with diluted H_2SO_4. Copper(I) chloride must always be covered by a layer of the acid solution. The solid is then washed four times with 10 mL of glacial acetic acid, three times with 15 mL of dry ethanol and finally six times with 8 mL of anhydrous ether. Due to its air instability, CuCl is stored inside the glove box.

2.2 Instruments

All the reactions under controlled atmosphere were conducted inside a MBraun Labstar glove box equipped with automatic pressure control and suitable for inorganic syntheses.

The infrared (IR) spectra were registered using a Perkin-Elmer SpectrumOne spectrometer between 4000 and 400 cm^{-1} using KBr as dispersing matrix.

The mono- and bidimensional nuclear magnetic resonance (NMR) spectra were collected at variable temperature employing Bruker Avance 300 and Avance 400 instruments operating respectively at 300.13 MHz and 400.13 MHz of protonic resonance. According to the solubility, the samples were prepared by dissolving the solids into $CDCl_3$ or DMSO-d_6. ^{1}H and ^{13}C NMR spectra are referred to the partially deuterated fraction of the solvent, itself referred to tetramethylsilane. ^{31}P NMR resonances are referred to 85% H_3PO_4 in water.

Melting points were registered employing a FALC 360 D instrument equipped with a camera. Conductivity measurements were recorded using a Radiometer Copenhagen CDM 83 instrument and they were interpreted according to the literature [34]. Electrochemical measurements, such as cyclic voltammetry and square voltammetry, were performed using an eDAQ ET014-199 instrument in sulfolane/0.04 M tetrabutylammonium hexafluorophoshate $[NBu_4][PF_6]$. Solvent and supporting electrolyte were used without further purification. The working electrode was a 1 mm glassy carbon disk ET074-1 while the counter one was a 1.6 mm-diameter Pt/Ti Titanium Wire Anode ET078-1. Both the electrodes belonged to the electrochemical kit provided by eDAQ. The couple Fc/Fc^{+} was used as internal standard and all the measurements were carried out at room temperature under argon atmosphere.

Absorption spectra in dimethylsulfoxide (DMSO) or dichloromethane were collected employing a Perkin-Elmer Lambda 35 spectrophotometer. The solvent was chosen according to the complex solubility and so the operating interval: for DMSO the wavelength range was between 265 and 700 nm, while for dichloromethane it was between 235 and 700 nm.

Preliminary emission spectra on solid samples were registered at room temperature between 400 and 1035 nm using an OceanOptics Flame T spectrophotometer paired with an optical fiber, an achromatic collimating lens and a long pass filter with cut-off

wavelength of 395 nm. To excite the samples a led source centred at 375 nm was employed.

PL and PLE spectra and lifetime decay curves were collected for solid samples with a Horiba Jobin Ybon Fluorolog-3 spectrometer. The instrument is equipped with a Xenon lamp as continuous excitation source and the operating wavelength is chosen thanks to a Czerny-Turner monochromator. As pulsing source, a led centred at 377 nm (SpectraLed) is used. Suitable long pass filters were placed in front of the acquisition systems. The detector is composed of a single monochromator iHR320 and a photomultiplier tube Hamamatsu R928. As regards the lifetime decays curves, a Multi-Channel Scaling (MCS) technique was employed.

UV LEDs VCC VAOL-5EUV8T4, characterized by maximum of emission at 385 nm and luminous intensity of 100 mcd, were purchased from RS Components and connected to a Keithley 2400 Source Meter.

Structural determination via X-Ray Diffraction (XRD) on single crystals was conducted at Vigo University in Spain.

2.3 DFT calculations

The ground-state geometry optimizations were carried out using the range-separated hybrid DFT functional ωB97X in combination with Alhrichs' split-valence basis set def2-SVP [35]. The relative energies of the excited states were obtained by carrying out TD-DFT (time-dependent DFT) calculations at the same theoretical level using the ground-state geometries. Selected excited states were optimized on changing the multiplicity of the compounds. Frontier molecular orbital energies were obtained from Hartree-Fock calculations using the basis set above described. The software used was Gaussian 09 [36].

2.4 Ligands syntheses

2.4.1 Monodentate ligands

2.4.1.1 Synthesis of N-Methylbenzotriazole, btz^{Me}

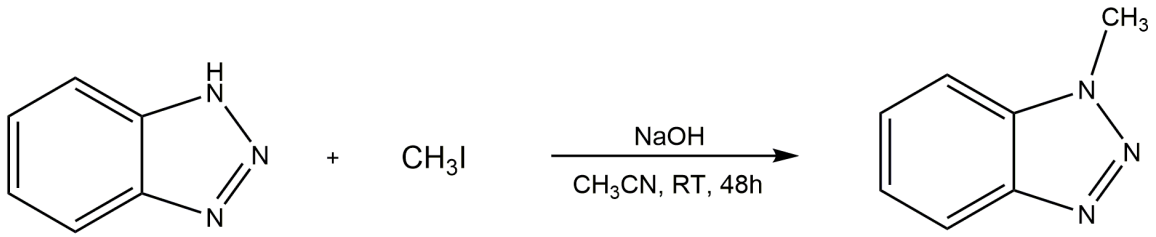

Scheme 1. Synthesis of N-methylbenzotriazole

The N-functionalized heterocycle was prepared according to a procedure reported in literature [37]. To a stirred solution containing 5.003 g of benzotriazole (42.0 mmol) and 75 mL of acetonitrile a solution of NaOH aq. (8 mL, 25%) was added. Another solution containing 3.2 mL of CH_3I (51.4 mmol) in 8 mL of CH_3CN was subsequently added. Then the reaction mixture was stirred for 48 hours under nitrogen atmosphere, concentrated under vacuum and the product was extracted four times with 25 mL of chloroform. The organic phase was washed twice with 25 mL of distilled water and dried with Na_2SO_4, filtrated and concentrated *in vacuo*. Isohexane was added to facilitate the precipitation of the product as a white solid. Yield: 60%.

2.4.1.2 Synthesis of 1-Methylindazole, ind^{Me}

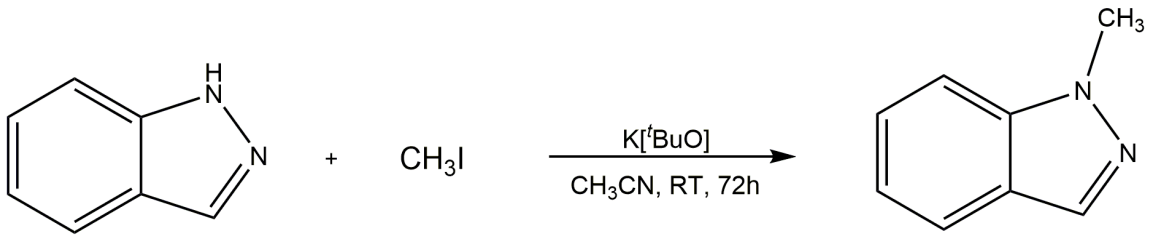

Scheme 2. Synthesis of N-methylindazole

To a frozen solution of indazole (1.181 g, 10.0 mmol) in 100 mL of acetonitrile, 1.121 g of K[^{t}BuO] (10.0 mmol) were added under nitrogen atmosphere. Once the stirred solution had reached room temperature (approx. 90 minutes), it was frozen again and 0.93 mL of CH_3I (15.0 mmol) were added. Then the mixture was stirred for 3 days, quenched with 20 mL of distilled water, concentrated *in vacuo* and extracted three times with 15 mL of diethyl ether. After it was dried with Na_2SO_4, the solution was filtered and concentrated using the rotary evaporator. A yellow oil was afforded but, as methylation could occur both in position 1 and 2, the two isomers were

separated via column chromatography (SiO_2, 1:1 isohexane:ethyl acetate). After the evaporation of the solvents, a brownish solid was afforded. Yield: 50%. Characterization data coincide with those reported using different procedures [38].

2.4.2 Bidentate ligands

2.4.2.1 Synthesis of 1,1'-carbonylbis-azole (azole = benzotriazole, indazole)

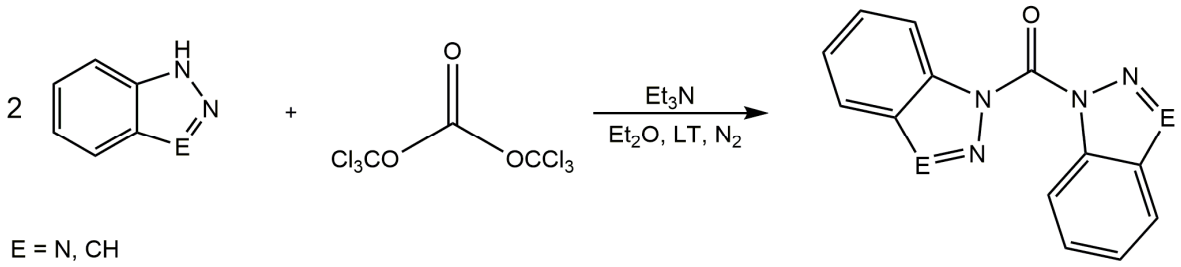

Scheme 3. Synthesis of 1,1'-carbonylbis-azoles

The reactions were conducted inside the glove box for safety reasons. In a jacketed reactor cooled down with liquid nitrogen 1.246 g of triphosgene (4.2 mmol) were placed and dissolved in 50 mL of dry diethyl ether. 3.5 mL of TEA (TEA = triethylamine; 25.2 mmol) were added, then 25.2 mmol of the chosen H-azole were slowly introduced into the reactor when the temperature had reached -70 °C. Particular attention had to be devoted to the temperature especially when indazole was involved in the synthesis.

The solution was left under stirring and allowed to slowly reach room temperature, then the work-up was conducted outside the glove box. Firstly, the white precipitate, mostly composed by the product and tetraethylammonium chloride, was filtered and dried *in vacuo*. The solid was then dissolved in dichloromethane and extracted with distilled water. The aqueous phase was washed three times with 15 mL of dichloromethane and the organic fractions were collected together and then dried with Na_2SO_4. The solution was filtered, and the solvent was concentrated *in vacuo* to give a brown oil, that was precipitated with ether to afford a white solid. Yield: 65% in both the cases. Characterization data of 1,1'-carbonylbis-benzotriazole coincide with those reported for the same compound obtained with different synthetic approaches [39]. A previous synthesis of 1,1'-carbonylbis-indazole based on phosgene as

reactant is reported in the literature, but characterization data are collected below for completeness [40].

Characterization of 1,1'-carbonylbis-indazole. ^{1}H NMR ($CDCl_3$, 298 K) δ 8.39 (s, 1H, indazole-CH), 8.32 (d, 1H, J_{HH} = 8.4 Hz, phenyl), 7.85 (d, 1H, J_{HH} = 8.0 Hz, phenyl), 7.65 (dd, 1H, J_{HH} = 7.2 Hz, J_{HH} = 8.4 Hz, phenyl), 7.45 (t, 1H, J_{HH} = 7.7 Hz, phenyl). IR (KBr, cm^{-1}): 1698 ν_{CO}.

2.4.2.2 Synthesis of 1,1'-bis(azolyl)phenylmethane [azolyl = benzotriazolyl, L = $CHPh(btz)_2$; azolyl = indazolyl, L = $CHPh(ind)_2$]

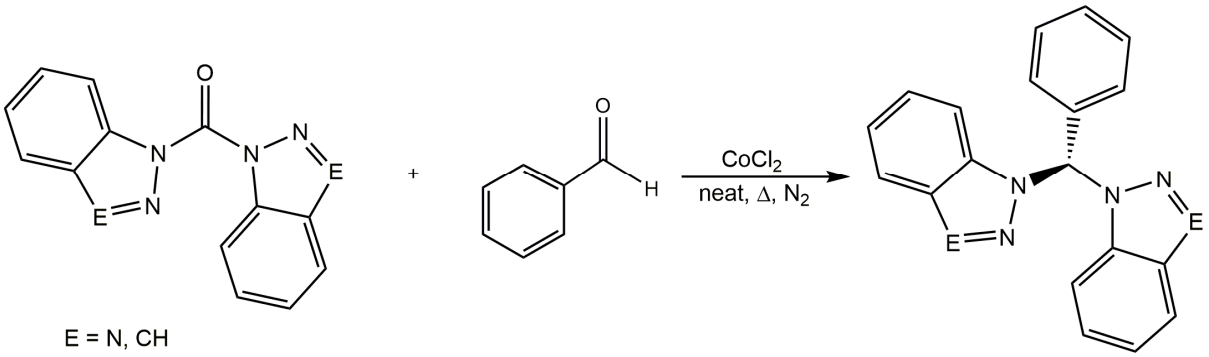

Scheme 4. Synthesis of 1,1'-bis(azolyl)phenylmethane ligands

The ligands were obtained on the basis of a general procedure reported in the literature [41]. The reaction was conducted in a Schlenk apparatus under nitrogen atmosphere and it was catalysed by anhydrous $CoCl_2$. In the Schlenk apparatus 2.0 mmol of 1,1'-carbonylbis-azole, 2.0 mmol of benzaldehyde (0.20 mL) and a catalytic amount (approx. 0.004 g) of $CoCl_2$ were added. The solids were heated to 150 °C until they melted, and the formation of CO_2 was observed. The solution was stirred at this temperature for 2 hours, then it was left to cool down. Once the mixture had reached room temperature, the solid was dissolved in dichloromethane and the solution was extracted with distilled water. The aqueous phase was subsequently washed three times with 15 mL of dichloromethane and, after all the organic fractions were collected, the solution was dried with Na_2SO_4. The organic phase was filtered, and the solvent was concentrated *in vacuo* to give a brown oil that was precipitated with ether to afford a white solid. Yield: 40%. Characterization data coincide with those reported for the same compounds prepared on the basis of different procedures [42].

2.4.3 Tridentate ligands

2.4.3.1 Synthesis of 1,1'-bis(benzotriazolyl)-pyridin-2-yl-methane, $CHPy(btz)_2$

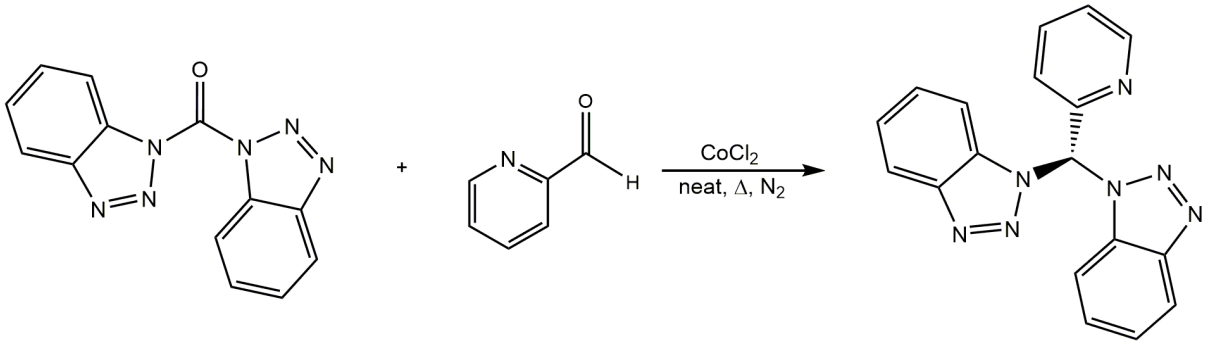

Scheme 5. Synthesis of 1,1'-bis(benzotriazolyl)-pyridin-2-yl-methane

The ligand was obtained on the basis of the method previously described for 1,1'-bis(benzotriazolyl)phenylmethane, using pyridine-2-carboxyaldehyde (2.0 mmol, 0.19 mL) as reactant. The temperature was kept at 85 °C to avoid decomposition. The product was extracted three times with 25 mL of hot cyclohexane and the yellow solution was concentrated by rotary evaporation. The slow cooling down of the mixture afforded crystals suitable to X-Ray diffraction as well. The brown oil was precipitated with diethyl ether to afford a light orange solid. Yield: 30%.

Characterization of 1,1'-bis(benzotriazolyl)-pyridin-2-yl-methane. ^{1}H NMR ($CDCl_3$, 298 K) δ 9.00 (s, 1H, CH), 8.66 (ddd, 1H, J_{HH} = 4.8 Hz, J_{HH} = 1.7 Hz, J_{HH} = 0.9 Hz, pyridine-H_6), 8.10 (dt, 2H, J_{HH} = 8.3 Hz, J_{HH} = 0.9 Hz, benzotriazole), 7.82 (td, 1H, J_{HH} = 7.8 Hz, J_{HH} = 1.7 Hz, pyridine-H_4), 7.67 (dt, 2H, J_{HH} = 8.4 Hz, J_{HH} = 1.0 Hz, benzotriazole), 7.49 (ddd, 2H, J_{HH} = 8.1 Hz, J_{HH} = 7.0 Hz, J_{HH} = 1.1 Hz, benzotriazole), 7.42 (dd, 1H, J_{HH} = 7.8 Hz, J_{HH} = 4.8 Hz, pyridine-H_5), 7.41 (dt, 2H, J_{HH} = 8.2 Hz, J_{HH} = 7.0 Hz, J_{HH} = 1.0 Hz, benzotriazole), 7.32 (ddd, 1H, J_{HH} = 7.8 Hz, J_{HH} = 1.7 Hz, J_{HH} = 0.9 Hz, pyridine-H_3). ^{13}C {^{1}H} NMR ($CDCl_3$, 298 K) δ 151.56 (ipso), 150.11 (py-C_6), 146.28 (ipso), 137.35 (py-C_4), 132.64 (ipso), 128.59 (btz), 124.78 (btz), 124.54 (py-C_5), 122.48 (py-C_3), 120.33 (btz), 110.68 (btz), 73.43 (CH). IR (KBr, cm^{-1}): 3060-2950 ν_{CH}; 1610-1430 $\nu_{C=C}$, $\nu_{C=N}$.

2.4.3.2 Synthesis of tris(benzotriazol-1-yl)methane, $CH(btz)_3$

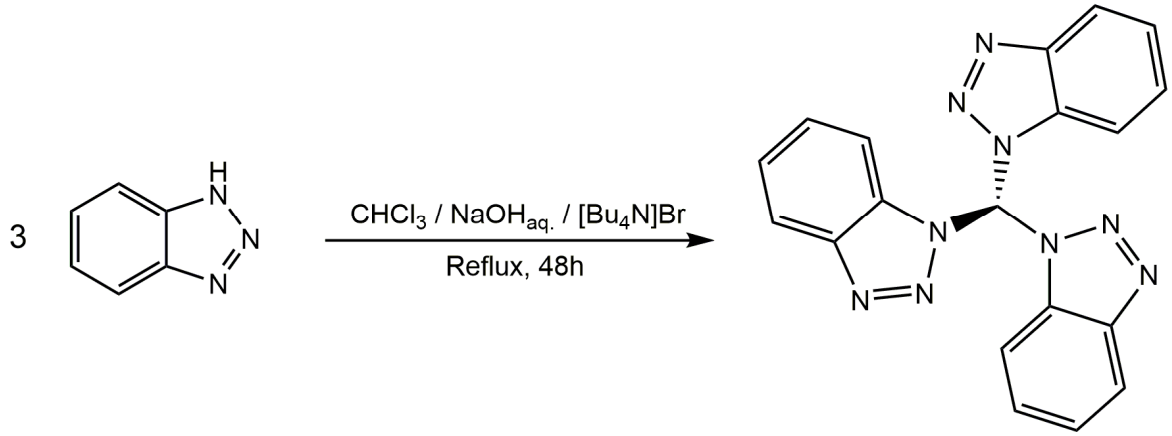

Scheme 6. Synthesis of tris(benzotriazol-1-yl)methane

The ligand was obtained following a procedure reported in literature [43]. To a heterogeneous mixture containing 5.956 g of benzotriazole (50.0 mmol) in 5 mL of $CHCl_3$, 5 mL of a concentrated solution of NaOH aq. 40% were added. As a phase transfer catalyst is required due to the insolubility between the organic and the aqueous phases, 0.160 g of $[Bu_4N]Br$ were added as well. The solution was heated under reflux for 48 hours and, once it had cooled down to room temperature, it was extracted twice with 5 mL of chloroform. The organic phase was washed five times with 5 mL of distilled water, dried with Na_2SO_4, filtrated and concentrated *in vacuo*. The oil was finally treated with methanol to afford the desired product as a white precipitate. Yield: 50%.

2.5 Precursors syntheses

2.5.1 Synthesis of $[Cu(BH_4)(PPh_3)_2]$

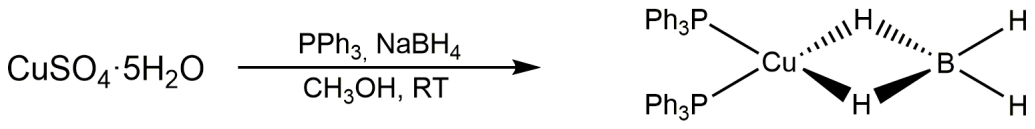

Scheme 7. Synthesis of $[Cu(BH_4)(PPh_3)_2]$

This precursor was prepared following a procedure reported in literature [44]. A stirred solution containing 0.500 g of copper(II) sulfate pentahydrate (2.0 mmol), 2.500 g of triphenylphosphine (9.5 mmol) and 100 mL of methanol was heated until

the dissolution of the solids. After the mixture had cooled down to room temperature, sodium borohydride (0.500 g, 13.2 mmol) was added in small amounts. The formation of H_2 was observed. The white precipitated was filtered and purified by dissolution in 20 mL of dichloromethane. After the filtration of the solution, 25 mL of methanol were added and CH_2Cl_2 was concentrated *in vacuo* until the precipitation of a white solid was observed. Quantitive yield.

2.5.2 Synthesis of [Cu(BH$_4$)(dppe)] [dppe = 1,2-bis(diphenylphosphino)ethane]

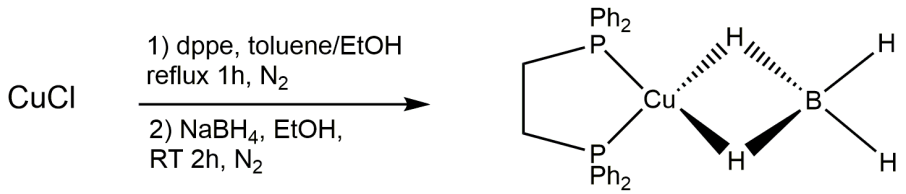

Scheme 8. Synthesis of [Cu(BH$_4$)(dppe)]

A stirred solution of CuCl (0.500 g, 5.0 mmol) and dppe (4.427 g, 11.1 mmol) in 40 mL of toluene was heated to reflux under nitrogen atmosphere for one hour. To facilitate the solubilization of the phosphine 15 mL of ethanol were added. After the mixture had cooled down to room temperature, a solution containing 0.401 g of $NaBH_4$ (10.6 mmol) in ethanol (10 mL) was added dropwise through a syringe and stirred for 2 hours. Then the solvent was evaporated under low pressure to afford an oil that later was dissolved in 20 mL dichloromethane. After the solution was filtered, diethyl ether was added to precipitate a solid that was purified by adding 20 mL of dichloromethane and 15 mL of ethanol. The low boiling solvent was removed by rotary evaporation and the complex precipitated from ethanol as a white solid. Yield: 30%.

2.5.3 Synthesis of $[Cu(NCCH_3)_4][BF_4]$

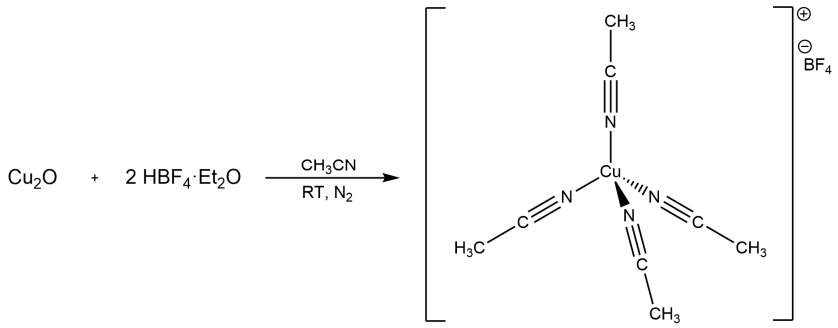

Scheme 9. Synthesis of $[Cu(NCCH_3)_4][BF_4]$

The complex was obtained following a procedure reported in literature [45]. Due to its air instability, the synthesis was conducted inside the glove box. To a stirred solution of 0.500 g of copper(I) oxide (3.5 mmol) in 20 mL of acetonitrile, 1.0 mL of $HBF_4 \cdot Et_2O$ was added. The evolution of the reaction was indicated by the dissolution of the red solid Cu_2O. After the disappearance of the solid, the acetonitrile was evaporated under reduced pressure to give a brownish solid that was purified. The precipitate was firstly dissolved in dichloromethane and then the solid impurities were eliminated by centrifuge. This procedure was repeated twice, and all the organic fractions were filtered on cotton and collected together. The solvent was concentrated under low pressure, the complex was precipitated with diethyl ether and stored inside the glove box. Yield: 60%.

2.6 Reactions of N-donor ligands with copper borohydride precursors

2.6.1 Synthesis of $[Cu(btz^{Me})(P\text{-}P)]_2[BF_4]_2$ [P-P = $(PPh_3)_2$ or dppe]

N-methylbenzotriazole (0.200 g, 1.5 mmol) was first protonated with $HBF_4 \cdot Et_2O$ (0.20 mL, 1.5 mmol) to afford the corresponding salt in 15 mL of diethyl ether. The solid formed was separated by filtration, dried *in vacuo* and added to a flask containing a stoichiometric quantity of solid $[Cu(BH_4)(PPh_3)_2]$ or $[Cu(BH_4)(dppe)]$. The mixture of solids was put under inert atmosphere and cooled at -196 °C by means of a liquid nitrogen bath. Dichloromethane (20 mL) was then slowly added by a syringe and the reaction mixture was allowed to slowly warm to room temperature. After stirring

overnight at room temperature, dichloromethane was evaporated at reduced pressure to afford an oil that was washed with diethyl ether. In the case of $[Cu(btz^{Me})(dppe)]_2[BF_4]_2$ the compound was isolated as powder after treatment with few mL of ethanol. Yield > 70% in both the cases.

Characterization of $[Cu(btz^{Me})(PPh_3)_2]_2[BF_4]_2$. ^{1}H NMR ($CDCl_3$, 298 K) δ 7.77 (d, 1H, J_{HH} = 8.7 Hz, btz^{Me}), 7.60-7.10 (m, 33H, btz^{Me} and PPh_3), 4.33 (s, 3H, btz^{Me}). ^{31}P {^{1}H} NMR ($CDCl_3$, 298 K) δ 0.88 (br). IR (KBr, cm^{-1}): 3050-2850 ν_{CH}; 1610-1410 $\nu_{C=C}$, $\nu_{C=N}$; 1100-990 ν_{BF4}. Λ_M (acetone, 298 K, MW 808 g mol^{-1}) 103 ohm^{-1}mol^{-1}cm^2. M.p. 90°C (dec.). UV-VIS (CH_2Cl_2, 298 K, nm) < 350, 257 (max), 268 (sh), 308 (sh). PL (solid, r.t., $\lambda_{excitation}$ = 375 nm, nm) 501 (sh), 518, 534, 550 (max), 566, 586, 607, 630 (sh), 656 (sh), 683 (sh), 714 (sh). PLE (solid, r.t., $\lambda_{emission}$ = 560 nm, nm) < 460, 387 (max). τ (solid, r.t., $\lambda_{excitation}$ = 377 nm, $\lambda_{emission}$ = 550 nm, μs): 30.

Characterization of $[Cu(btz^{Me})(dppe)]_2[BF_4]_2$. ^{1}H NMR ($CDCl_3$, 298 K) δ 8.00-7.10 (m, 24H, btz^{Me} and dppe), 4.32 (s, 3H, btz^{Me}), 2.48 (m, 4H, dppe). ^{31}P {^{1}H} NMR ($CDCl_3$, 208 K) δ 7.95 (br). IR (KBr, cm^{-1}): 3050-2850 ν_{CH}; 1610-1410 $\nu_{C=C}$, $\nu_{C=N}$; 1100-990 ν_{BF4}. Λ_M (acetone, 298 K, MW 682 g mol^{-1}) 124 ohm^{-1}mol^{-1}cm^2. M.p. 155°C. UV-VIS (CH_2Cl_2, 298 K, nm) < 360, 263 (max), 270 (sh), 315 (sh). PL (solid, r.t., $\lambda_{excitation}$ = 375 nm, nm) 510 (sh), 526 (sh), 546, 561, 579 (max), 599, 620, 643 (sh), 669 (sh), 695 (sh). PLE (solid, r.t., $\lambda_{emission}$ = 585 nm, nm) < 460, 395 (sh), 353 (max). τ (solid, r.t., $\lambda_{excitation}$ = 377 nm, $\lambda_{emission}$ = 579 nm, μs): 33.

2.6.2 Synthesis of $[Cu\{CHPh(btz)_2\}(P\text{-}P)][BF_4]$ [P-P = $(PPh_3)_2$ or dppe]

The compounds were prepared following the procedure above described for $[Cu(btz^{Me})(P\text{-}P)]_2[BF_4]_2$, with the exception that $CHPh(btz)_2$ (one equivalent with respect to the copper precursor) was used as N-donor ligand and it was protonated with $HBF_4{\cdot}Et_2O$ in dichloromethane. Yield > 70% in both the cases.

Characterization of $[Cu\{CHPh(btz)_2\}(PPh_3)_2][BF_4]$. ^{1}H NMR ($CDCl_3$, 298 K) δ 9.17 (s, 1H, CH; ^{13}C HSQC 65.86), 8.40-8.00 (m, 4H, btz), 7.90-6.95 (m, 35H, Ph and PPh_3). ^{31}P {^{1}H} NMR ($CDCl_3$, 208 K) δ 0.08 (br). IR (KBr, cm^{-1}): 3100-2850 ν_{CH}; 1600-1430 $\nu_{C=C}$, $\nu_{C=N}$; 1170-1000 ν_{BF4}. Λ_M (acetone, 298 K, MW 1001 g mol^{-1}) 142 ohm^{-1}mol^{-}

$^{1}cm^{2}$. M.p. 105°C (dec.). UV-VIS (CH_2Cl_2, 298 K) < 310, 255 (max), 262 (sh), 274 (sh), 311 (sh). PL (solid, r.t., $\lambda_{excitation}$ = 375 nm, nm) 518 (sh), 533 (sh), 550, 565 (max), 582, 601, 623 (sh), 646 (sh), 671 (sh), 697 (sh). PLE (solid, r.t., $\lambda_{emission}$ = 586 nm, nm) < 460. τ (solid, r.t., $\lambda_{excitation}$ = 377 nm, $\lambda_{emission}$ = 565 nm, μs): 22.

Characterization of [Cu{CHPh(btz)$_2$}(dppe)][BF$_4$]. ^{1}H NMR ($CDCl_3$, 208 K) δ 9.11 (s, 1H, CH), 8.40-6.60 (m, 29H, btz and Ph and dppe), 2.38 (s, br, 4H, dppe). ^{31}P {^{1}H} NMR ($CDCl_3$, 208 K) δ 7.72 (br). IR (KBr, cm^{-1}): 3100-2800 ν_{CH}; 1600-1430 $\nu_{C=C}$, $\nu_{C=N}$; 1170-1000 ν_{BF4}. Λ_M (acetone, 298 K, MW 875 g mol^{-1}) 104 $ohm^{-1}mol^{-1}cm^{2}$. M.p. 100°C (dec.). UV-VIS (CH_2Cl_2, 298 K) < 380, 254 (max), 264 (sh), 269 (sh), 317 (sh). PL (solid, r.t., $\lambda_{excitation}$ = 375 nm, nm) 526 sh, 541, 558, 573 (max), 591, 610, 629, 650, 675. PLE (solid, r.t., $\lambda_{emission}$ = 600 nm, nm) < 450.

2.6.3 Synthesis of [Cu{CHPh(ind)$_2$}(PPh$_3$)$_2$][BF$_4$]

The preparation of the title compound was carried out following the procedure above described for [Cu{CHPh(btz)$_2$}(PPh$_3$)$_2$][BF$_4$], using CHPh(ind)$_2$ as ligand. Yield > 70%.

Characterization of [Cu{CHPh(ind)$_2$}(PPh$_3$)$_2$][BF$_4$]. ^{1}H NMR ($CDCl_3$, 298 K) δ 8.66 (s, 1H, CH), 8.15 (d, br, 2H, J_{HH} = 8.1 Hz, ind), 7.95 (s, 2H, ind), 7.75-7.00 (m, 35H, Ph and PPh_3), 6.95-6.80 (m, br, 4H, ind), 6.41 (m, br, 2H, ind). ^{31}P {^{1}H} NMR ($CDCl_3$, 298 K) δ 0.02 (br). IR (KBr, cm^{-1}): 3050-2850 ν_{CH}; 1620-1430 $\nu_{C=C}$, $\nu_{C=N}$; 1160-990 ν_{BF4}. Λ_M (acetone, 298 K, MW 999 g mol^{-1}) 193 $ohm^{-1}mol^{-1}cm^{2}$. M.p. 75°C (dec.). UV-VIS (CH_2Cl_2, 298 K) < 320, 257 (max), 275 (sh), 281 (sh), 287 (sh), 293 (sh), 315 (sh). PL (solid, r.t., $\lambda_{excitation}$ = 375 nm, nm) 448, 498, 509 (max), 525, 539. PLE (solid, r.t., $\lambda_{emission}$ = 560 nm, nm) 365 (max).

2.6.4 Synthesis of [Cu{CHPy(btz)$_2$}(PPh$_3$)][BF$_4$]

The preparation of the title compound was carried out following the procedure above described for [Cu{CHPh(btz)$_2$}(PPh$_3$)$_2$][BF$_4$], using CHPy(btz)$_2$ as ligand. Yield > 70%.

Characterization of [Cu{CHPy(btz)$_2$}(PPh$_3$)][BF$_4$]. ^{1}H NMR (DMSO-d$_6$, 298 K) δ 9.85 (s, 1H, CH), 8.58 (ddd, 1H, J_{HH} = 4.8 Hz, J_{HH} = 1.8 Hz, J_{HH} = 0.9 Hz, py-H$_6$), 8.13 (dt, 2H, J_{HH} = 8.3 Hz, J_{HH} = 1.0 Hz, btz), 7.97 (td, J_{HH} = 7.7 Hz, J_{HH} = 1.8 Hz, py-H$_4$), 7.75 (dt, 2H, J_{HH} = 8.4 Hz, J_{HH} = 1.0 Hz, btz), 7.70-7.20 (m, 19H, py and btz and PPh$_3$). ^{31}P{^{1}H} NMR (DMSO-d$_6$, 298 K) δ -3.81 (br). IR (KBr, cm^{-1}): 3060-2850 ν_{CH}; 1620-1430 $\nu_{C=C}$, $\nu_{C=N}$; 1170-1000 ν_{BF4}. Λ_M (acetone, 298 K, MW 740 g mol^{-1}) 151 ohm^{-1}mol^{-1}cm^2. M.p. 80°C (dec.). UV-VIS (CH_2Cl_2, 298 K) < 350, 262 (max), 319 (sh). PL (solid, r.t., $\lambda_{excitation}$ = 375 nm, nm) 558 (max, FWHM = 5200 cm^{-1}). PLE (solid, r.t., $\lambda_{emission}$ = 567 nm, nm) 440 (max).

2.7 Reactions of N-donor ligands with copper acetonitrile precursor

2.7.1 Synthesis of [Cu(ind^{Me})(PPh$_3$)$_2$][BF$_4$] and [Cu(ind^{Me})(dppe)][BF$_4$]

A solution containing 0.472 g of [Cu(NCCH$_3$)$_4$][BF$_4$] (1.5 mmol) and 0.198 g of ind^{Me} (1.5 mmol) in dry dichloromethane (20 mL) was stirred overnight at room temperature, then the chosen phosphine was added (3.0 mmol for PPh$_3$ and 1.5 mmol for dppe) and the mixture was stirred again at room temperature overnight. To isolate the product, the solvent was evaporated under low pressure and the solid was precipitated by adding ether dropwise to the oil dissolved in the minimum volume of ethanol. Yield > 40% in both the cases.

Characterization of [Cu(ind^{Me})(PPh$_3$)$_2$][BF$_4$]. ^{1}H NMR ($CDCl_3$, 298 K) δ 8.21 (s, 1H, ind^{Me}), 7.79 (dt, 1H, J_{HH} = 8.3 Hz, J_{HH} = 1.0 Hz, ind^{Me}), 7.55-7.20 (m, 33H, ind^{Me} and PPh$_3$), 3.98 (s, 3H, ind^{Me}). ^{31}P{^{1}H} NMR ($CDCl_3$, 213 K) δ -0.55 (br). IR (KBr, cm^{-1}): 3050-2850 ν_{CH}; 1650-1430 $\nu_{C=C}$, $\nu_{C=N}$; 1120-990 ν_{BF4}. Λ_M (acetone, 298 K, MW 806 g mol^{-1}) 170 ohm^{-1}mol^{-1}cm^2. M.p. 135°C (dec.). UV-VIS (CH_2Cl_2, 298 K, nm) < 320, 257 (max), 290 (sh), 296 (sh), 303 (sh), 319 (sh). PL (solid, r.t., $\lambda_{excitation}$ = 323 nm, nm) 440, 470 (max), 502, 538. PLE (solid, $\lambda_{emission}$ = 505 nm, nm) < 370, 321 (max).

Characterization of [Cu(ind^{Me})(dppe)][BF$_4$]. ^{1}H NMR ($CDCl_3$, 298 K) δ 8.20 (s, 1H, ind^{Me}), 7.77 (dt, 1H, J_{HH} = 8.2 Hz, J_{HH} = 1.0 Hz, ind^{Me}), 7.70-7.10 (m, 23H, ind^{Me} and PPh$_3$), 4.16 (s, 3H, ind^{Me}). ^{31}P{^{1}H} NMR ($CDCl_3$, 213 K) δ 8.07 (br). IR (KBr, cm^{-1}): 3050-2860 ν_{CH}; 1620-1430 $\nu_{C=C}$, $\nu_{C=N}$; 1160-1000 ν_{BF4}. Λ_M (acetone, 298 K, MW 681

g mol^{-1}) 146 ohm^{-1}mol^{-1}cm^2. M.p. 90°C (dec.). UV-VIS (CH_2Cl_2, 298 K, nm) < 330, 260, 265 (max), 271 (sh), 281 (sh), 303 (sh), 317 (sh). PL (solid, r.t., $\lambda_{excitation}$ = 375 nm, nm) 446, 493 (max).

2.7.2 Synthesis of [Cu{CHPh(btz)$_2$}$_2$][BF$_4$] and [Cu{CHPh(ind)$_2$}$_2$][BF$_4$]

To a solution of 1.5 mmol of [Cu(NCCH$_3$)$_4$][BF$_4$] (0.472 g) in 50 mL of dichloromethane, the ligand CHPh(btz)$_2$ or CHPh(ind)$_2$ (3.0 mmol) was added and the mixture was stirred inside the glove box overnight. The solid that slowly separated from CH_2Cl_2 was then filtered, washed and dried *in vacuo*. Yield > 60% in both the cases.

Characterization of [Cu{CHPh(btz)$_2$}$_2$][BF$_4$]. ^{1}H NMR (DMSO-d$_6$, 298 K) δ 9.77 (s, 1H, CH), 8.14 (d, 2H, J_{HH} = 8.0 Hz, btz), 7.76 (d, 2H, J_{HH} = 8.0 Hz, btz), 7.60 (t, 2H, J_{HH} = 8.0 Hz, btz), 7.55-7.40 (m, 5H, btz and Ph), 7.24 (m, 2H, Ph). IR (KBr, cm^{-1}): 3100-2850 ν_{CH}; 1610-1450 $\nu_{C=C}$, $\nu_{C=N}$; 1160-1030 ν_{BF4}. Λ_M (CH_3NO_2, 298 K, MW 803 g mol^{-1}) 102 ohm^{-1}mol^{-1}cm^2. M.p. 205°C (dec.). UV-VIS (DMSO, 298 K, nm) < 400, 284 (max), 310 (sh). PL (solid, r.t., $\lambda_{excitation}$ = 375 nm, nm) 588 (max, FWHM = 4100 cm^{-1}). PLE (solid, $\lambda_{emission}$ = 600 nm, nm) < 470, 352 (max). τ (solid, r.t., $\lambda_{excitation}$ = 377 nm, $\lambda_{emission}$ = 588 nm, μs): 25.

Characterization of [Cu{CHPh(ind)$_2$}$_2$][BF$_4$]. ^{1}H NMR (DMSO-d$_6$, 338 K) δ 9.23 (s, br, 1H, CH), 8.18 (s, br, 2H, ind), 8.00-7.70 (m, br, 5H, arom.), 7.70-7.15 (m, 7H, arom.), 6.78 (m, br, 2H, arom.). ^{1}H NMR (DMSO-d$_6$, 338 K) δ 8.99 (s, 1H, CH), 8.04 (s, 2H, ind), 7.94 (d, 2H, J_{HH} = 8.6 Hz, ind), 7.82 (d, 2H, J_{HH} = 8.0 Hz, ind), 7.55-7.40 (m, 5H, arom.), 7.24 (t, 2H, J_{HH} = 7.7 Hz, arom.), 6.97 (m, br, 2H, arom.). IR (KBr, cm^{-1}): 3050-2850 ν_{CH}; 1620-1450 $\nu_{C=C}$, $\nu_{C=N}$; 1180-1050 ν_{BF4}. Λ_M (CH_3NO_2, 298 K, MW 799 g mol^{-1}) 113 ohm^{-1}mol^{-1}cm^2. M.p. 235°C (dec.). UV-VIS (DMSO, 298 K, nm) < 410, 291 (max), 298 (sh), 311 (sh). PL (solid, r.t., $\lambda_{excitation}$ = 375 nm, nm) 571 (max, FWHM = 4600 cm^{-1}). PLE (solid, $\lambda_{emission}$ = 600 nm, nm) < 450, 389 (max). τ (solid, r.t., $\lambda_{excitation}$ = 377 nm, $\lambda_{emission}$ = 571 nm, μs): 31.

2.7.3 Synthesis of [Cu{CHPy(btz)$_2$}][BF$_4$]

The reaction was carried out as described before for [Cu{CHPh(btz)$_2$}$_2$][BF$_4$], with the exception that a 1:1 stoichiometric amount of the ligand CHPy(btz)$_2$ (0.491 g, 1.5 mmol) was used. Yield > 65%.

Characterization of [Cu{CHPy(btz)$_2$}][BF$_4$]. ^{1}H NMR (DMSO-d$_6$, 298 K) δ 9.84 (s, 1H, CH), 8.57 (s, br, 1H, py-H$_6$), 8.12 (d, 2H, J_{HH} = 8.2 Hz, btz), 7.96 (t, 1H, J_{HH} = 7.4 Hz, py-H$_4$), 7.74 (d, 2H, J_{HH} = 8.1 Hz, btz), 7.65-7.40 (m, 5H, btz and py), 7.34 (d, 1H, J_{HH} = 7.9 Hz, py-H$_3$). IR (KBr, cm^{-1}): 3100-2850 ν_{CH}; 1600-1440 $\nu_{C=C}$, $\nu_{C=N}$; 1150-1060 ν_{BF4}. Λ_M (CH_3NO_2, 298 K, MW 478 g mol^{-1}) 108 ohm^{-1}mol^{-1}cm^2. M.p. 210°C (dec.). UV-VIS (DMSO, 298 K, nm) < 450, 284 (max), 310 (sh). PL (solid, r.t., $\lambda_{excitation}$ = 375 nm, nm) 537 (max).

2.8 Reactions between CuBr and N-donor ligands

2.8.1 Synthesis of [CuBr{CHPh(btz)$_2$}]$_x$

Due to the air instability of the precursor, the synthesis was carried out inside the glove box. To a solution of 1.0 mmol of CuBr (0.143 g) in 50 mL of dichloromethane, 1.0 mmol of CHPh(btz)$_2$ (0.326 g) was added and the mixture was stirred overnight. A yellow solid precipitated from the solution, which was filtered, washed with dichloromethane and dried under low pressure. Yield > 60%.

Characterization of [CuBr{CHPh(btz)$_2$}]$_x$. ^{1}H NMR (DMSO-d$_6$, 298 K) δ 9.77 (s, 1H, CH), 8.14 (d, 2H, J_{HH} = 8.0 Hz, btz), 7.76 (d, 2H, J_{HH} = 8.0 Hz, btz), 7.60 (t, 2H, J_{HH} = 8.0 Hz, btz), 7.55-7.40 (m, 5H, btz and Ph), 7.24 (m, 2H, Ph). IR (KBr, cm^{-1}): 3090-2850 ν_{CH}; 1610-1450 $\nu_{C=C}$, $\nu_{C=N}$. Λ_M (DMSO, 298 K, MW 470 g mol^{-1}) 31 ohm^{-1}mol^{-1}cm^2. M.p. 130°C (dec.). UV-VIS (DMSO, 298 K, nm) < 490, 283 (max), 314 (sh), 401 (sh). PL (solid, r.t., $\lambda_{excitation}$ = 375 nm, nm) 616 (max, FWHM = 3900 cm^{-1}). PLE (solid, $\lambda_{emission}$ = 645 nm, nm) < 470, 388, 312 (max).

2.8.2 Synthesis of [CuBr{CHPy(btz)$_2$}]

The synthesis was carried out as described above for [CuBr{CHPh(btz)$_2$}], using CHPy(btz)$_2$ (0.327 g, 1.0 mmol) as ligand. Yield > 70%.

Characterization of [CuBr{CHPy(btz)$_2$}]. ^{1}H NMR (DMSO-d$_6$, 298 K) δ 9.84 (s, 1H, CH), 8.57 (d, 1H, J_{HH} = 4.9 Hz, py-H$_6$), 8.12 (d, 2H, J_{HH} = 8.2 Hz, btz), 7.96 (td, 1H, J_{HH} = 7.9 Hz, J_{HH} = 1.4 Hz, py-H$_4$), 7.74 (d, 2H, J_{HH} = 8.1 Hz, btz), 7.60 (t, 2H, J_{HH} = 7.3, btz), 7.55 (dd, 1H, J_{HH} = 7.9 Hz, J_{HH} = 4.9 Hz, py-H$_5$), 7.47 (t, 2H, J_{HH} = 7.8 Hz, btz), 7.34 (d, 1H, J_{HH} = 7.9 Hz, py-H$_3$). ^{13}C {^{1}H} NMR (DMSO-d$_6$, 298 K) δ 152.09 (ipso), 150.00 (py-C$_6$), 145.71 (ipso), 138.40 (py-C$_4$), 133.14 (ipso), 129.09 (btz), 125.41 (btz), 125.28 (py-C$_5$), 123.33 (py-C$_3$), 120.11 (btz), 111.72 (btz), 72.57 (CH). IR (KBr, cm^{-1}): 3090-2900 ν_{CH}; 1610-1450 $\nu_{C=C}$, $\nu_{C=N}$. Λ_M (DMSO, 298 K, MW 471 g mol^{-1}) 23 ohm^{-1}mol^{-1}cm^2. M.p. 95°C (dec.). UV-VIS (DMSO, 298 K, nm) < 500, 281 (max), 317 (sh), 423 (sh). PL (solid, r.t., $\lambda_{excitation}$ = 375 nm, nm) 600 (max). PLE (solid, $\lambda_{emission}$ = 600 nm, nm) < 450, 368, 314 (max).

2.8.3 Synthesis of [CuBr{CH(btz)$_3$}]

The synthesis was carried out as described above for [CuBr{CHPy(btz)$_2$}], using CH(btz)$_3$ (0.317 g, 1.0 mmol) as ligand. Yield > 70%.

Characterization of [CuBr{CH(btz)$_3$}]. ^{1}H NMR (DMSO-d$_6$, 298 K) δ 11.28 (s, 1H, CH), 8.23 (d, 3H, J_{HH} = 8.3 Hz, btz), 7.63 (t, 3H, J_{HH} = 7.7 Hz, btz), 7.53 (m, 6H. btz). ^{13}C {^{1}H} NMR (DMSO-d$_6$, 298 K) δ 146.11 (ipso), 132.41 (ipso), 130.13 (btz), 126.09 (btz), 120.61 (btz), 111.14 (btz), 77.63 (CH). IR (KBr, cm^{-1}): 3090-2900 ν_{CH}; 1610-1450 $\nu_{C=C}$, $\nu_{C=N}$. PL (solid, r.t., $\lambda_{excitation}$ = 375 nm, nm) 599 (max, FWHM = 3500 cm^{-1}). PLE (solid, $\lambda_{emission}$ = 614 nm, nm) < 460, 394, 317 (max). τ (solid, r.t., $\lambda_{excitation}$ = 377 nm, $\lambda_{emission}$ = 599 nm, μs): 19.

3. Results and discussion

The studies on new luminescent Cu(I) complexes started trying to prepare mixed-ligand coordination compounds with phosphines and N-methylbenzotriazole (btz^{Me}) in the coordination sphere. After several attempts, compounds having proposed formula $[Cu(btz^{Me})(P\text{-}P)]_2[BF_4]_2$, where P-P is $(PPh_3)_2$ or dppe, were isolated by reacting at low temperature the borohydride precursors $[Cu(BH_4)(P\text{-}P)]$ with one equivalent of the conjugate acid of btz^{Me} (see Scheme 10). This last species was obtained by reacting btz^{Me} with $HBF_4{\cdot}Et_2O$.

Characterization data agree with the proposed general formula. Conductivity data support the 1:1 Cu/BF_4 ratio. IR spectra clearly indicate the disappearance of the borohydride ligands and show signals attributable to btz^{Me} superimposed to those of the coordinated phosphines. ^1H NMR spectra show resonances attributable to btz^{Me}, particularly diagnostic being the singlet around 4.30 ppm related to the N-Me moiety. The presence of the phosphines is confirmed by the aromatic resonances in the ^1H NMR spectra and, in the case of the dppe derivative, by the signal centred at 2.48 ppm attributable to the P-bonded methylene fragments. Only one broad resonance is present in the ^{31}P $\{^1H\}$ NMR spectra, suggesting fluxional behaviour, and in the case of $[Cu(btz^{Me})(dppe)]_2[BF_4]_2$ the ^{31}P NMR resonance can be detected only on cooling the sample. The presence of the counter-anion is highlighted by the B-F stretchings in the IR range 1100-990 cm^{-1} and by a quintet ($^1J_{BF}$ = 0.9 Hz) in the ^{11}B NMR spectra. The NMR spectra of $[Cu(btz^{Me})(PPh_3)_2]_2[BF_4]_2$ are reported as example in Figure 23. The bridging mode of btz^{Me} depicted in Scheme 10 is proposed on the basis of literature outcomes concerning this class of ligands coordinated to Cu(I) [31, 46], but we were unable to grow crystals suitable for X-ray diffractions and therefore confirm the structure.

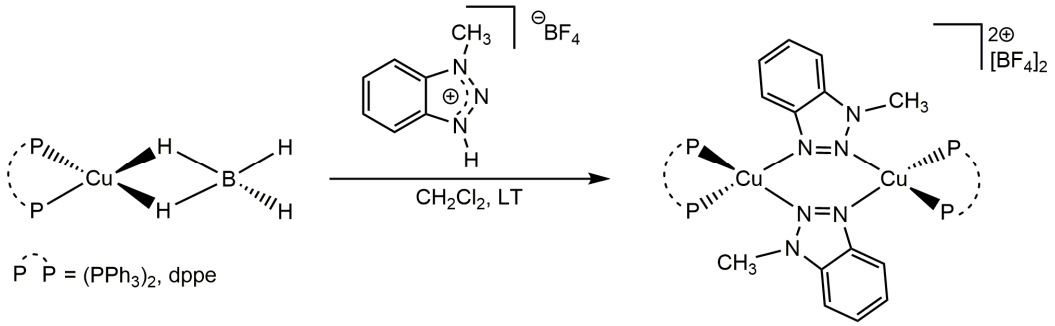

Scheme 10. Synthesis of $[Cu(btz^{Me})(P\text{-}P)]_2[BF_4]_2$ [P-P = $(PPh_3)_2$; dppe]

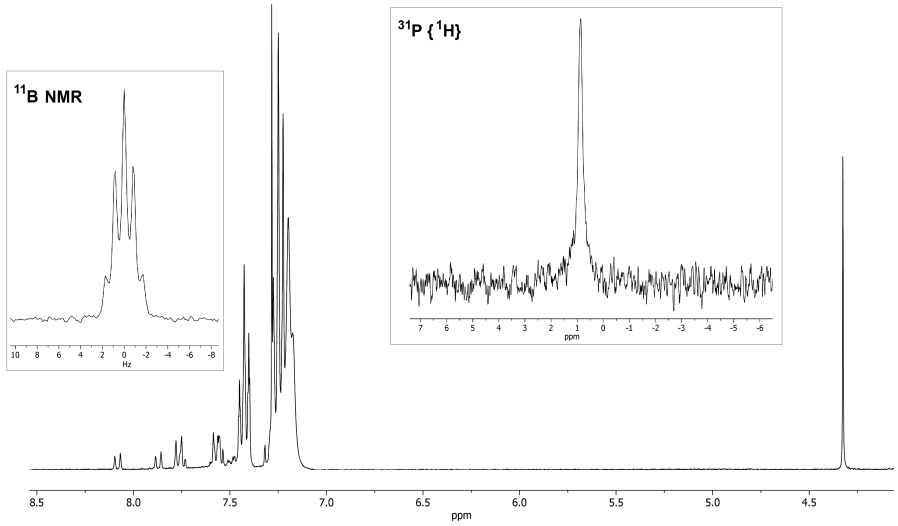

Figure 23. ^{1}H NMR, ^{31}P {^{1}H} and ^{11}B NMR of $[Cu(btz^{Me})(PPh_3)_2]_2[BF_4]_2$ ($CDCl_3$, 298 K).

The complexes are characterized by absorptions for wavelengths below 350 nm in CH_2Cl_2 solution. Excitation of solid samples with near-UV light caused bright yellow emissions, centred between 550 and 579 nm, as observable in the PL spectra reported in Figure 24. The luminescence is not maintained in solution. The features of the emission bands are influenced by the choice of the phosphines. In particular, the emission of the dppe derivative is red-shifted by about 30 nm with respect to the corresponding PPh_3 complex. Moreover, the intensity of the emission is lower for the dppe compound under the same experimental conditions. This last result is tentatively attributable to the lower steric bulk of dppe with respect to two triphenylphosphines, that could facilitate the distortion of the coordination sphere of the compound moving from the ground- to the excited-state. The ground-state vibrational structure of the complexes can be detected in the emission bands, with peaks and shoulders separated by about 590 cm^{-1}, in agreement with bending of the benzotriazole skeleton. PLE measurements (see Figure 24) indicate that the yellow luminescence can be achieved by excitation in all the ultraviolet range, the near-UV in particular. The large Stokes shifts, the wide emission bands showing the vibrational structure of the coordinated btz^{Me} and the relatively long luminescence lifetimes, around 30 μs, suggest that the emissions of the complexes have ^{3}MLCT nature.

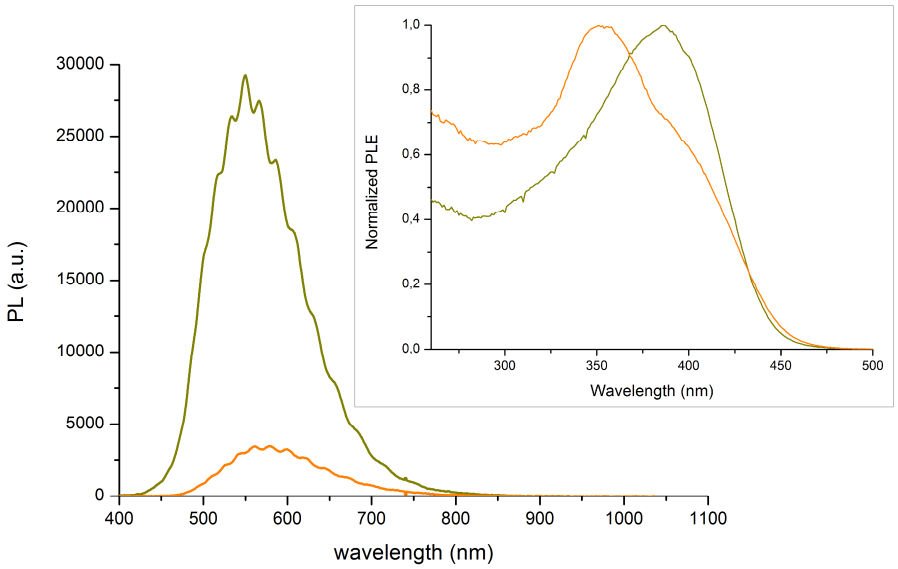

Figure 24. PL ($\lambda_{excitation}$ = 375 nm) and normalized PLE spectra of $[Cu(btz^{Me})(PPh_3)_2]_2[BF_4]_2$ (dark yellow line) and $[Cu(btz^{Me})(dppe)]_2[BF_4]_2$ (orange line). Solid samples, r.t.

Attempts to extend the above described synthetic approach to the ligand N-methylindazole (ind^{Me}) were unsuccessful. Mixed-ligand complexes having proposed formulae $[Cu(ind^{Me})(PPh_3)_2][BF_4]$ and $[Cu(ind^{Me})(dppe)][BF_4]$ were instead isolated by the stepwise reaction of the precursor $[Cu(NCCH_3)_4][BF_4]$ with ind^{Me} and the proper phosphine in dichloromethane. Despite the fact that characterization data are not sufficient to unambiguously define the structure of the complexes, conductivity data support the proposed formulae. The presence of both N- and P-donor ligands is confirmed by the IR and NMR spectra. In particular, besides the N-bonded methyl resonance between 3.98 and 4.16 ppm, the signal related to the CH fragment of the five-membered indazole ring can be detected around 8.20 ppm. The phosphine resonances closely resemble those previously described for the btz^{Me} complexes, but the fluxional behaviour in the ^{31}P NMR spectra appears more accentuated. As examples, the spectra of $[Cu(ind^{Me})(dppe)][BF_4]$ are shown in Figure 25.

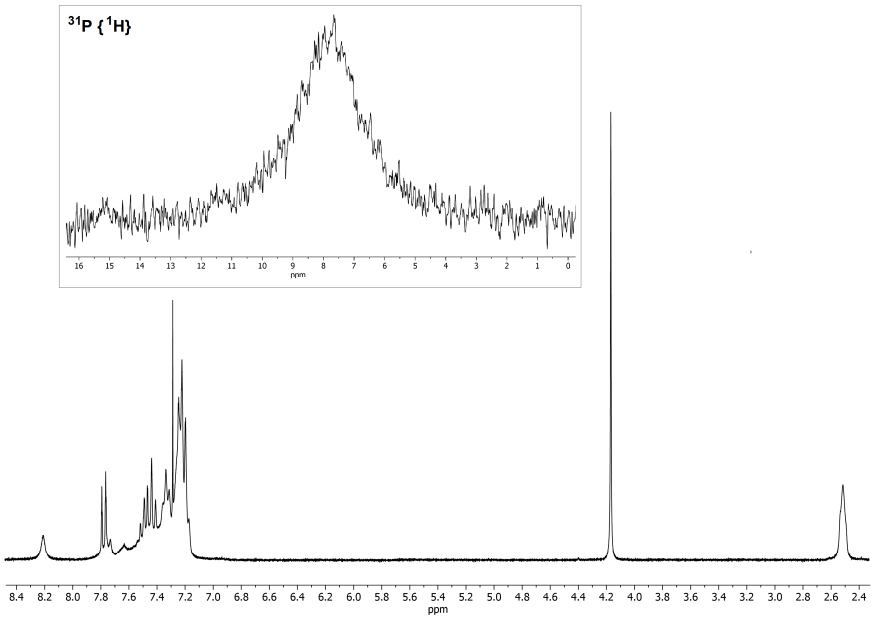

Figure 25. ^{1}H NMR (328 K) and ^{31}P $\{^{1}H\}$ NMR (213 K) of $[Cu(ind^{Me})(dppe)][BF_4]$ in $CDCl_3$.

Despite the fact that the absorption features of $[Cu(ind^{Me})(dppe)][BF_4]$ in CH_2Cl_2 are similar to those of the analogous benzotriazole derivatives, the solid-state luminescence is markedly different. The emission upon excitation with near-UV light is much weaker and, more important, it is meaningfully blue-shifted, with maxima centred between 470 and 493 nm (see for instance Figure 26). The scarce luminescence can be in part explained on considering the limited excitation range. As observable for instance in the PLE spectrum reported in Figure 26, the emission is associated to excitation with wavelengths below 370 nm.

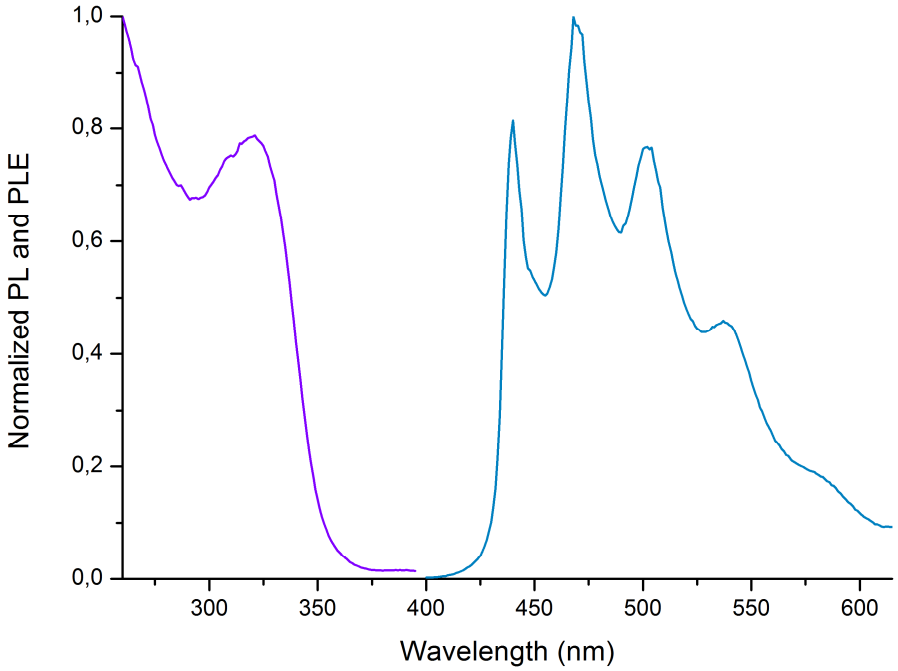

Figure 26. Normalized PL ($\lambda_{excitation}$ = 323 nm, light blue line) and PLE ($\lambda_{emission}$ = 505 nm, violet line) spectra of $[Cu(ind^{Me})(PPh_3)_2][BF_4]$. Solid samples, r.t.

It appears that the formal replacement of a nitrogen atom with a CH fragment in the five-membered ring of the heterocycle skeleton causes a shift to higher energies of the excitation and emission bands. This experimental outcome can be explained on supposing that the metal-to-ligand charge transfer towards coordinated ind^{Me} ligand requires more energy with respect to btz^{Me}. This hypothesis was supported by electrochemical measurements on the two free ligands. In the case of btz^{Me} an irreversible reduction peak was detected at -2.8 V (vs. Fc/Fc^+) in sulfolane solution, clearly highlighted by the square wave voltammogram of the solution (see Figure 27). The signal around -0.7 V is tentatively attributable to the corresponding oxidation process, and the redox process of btz^{Me} appears to be therefore irreversible [47]. The reduction of ind^{Me} under the same experimental conditions was not detected, probably because it takes place at more negative potentials and outside the available range.

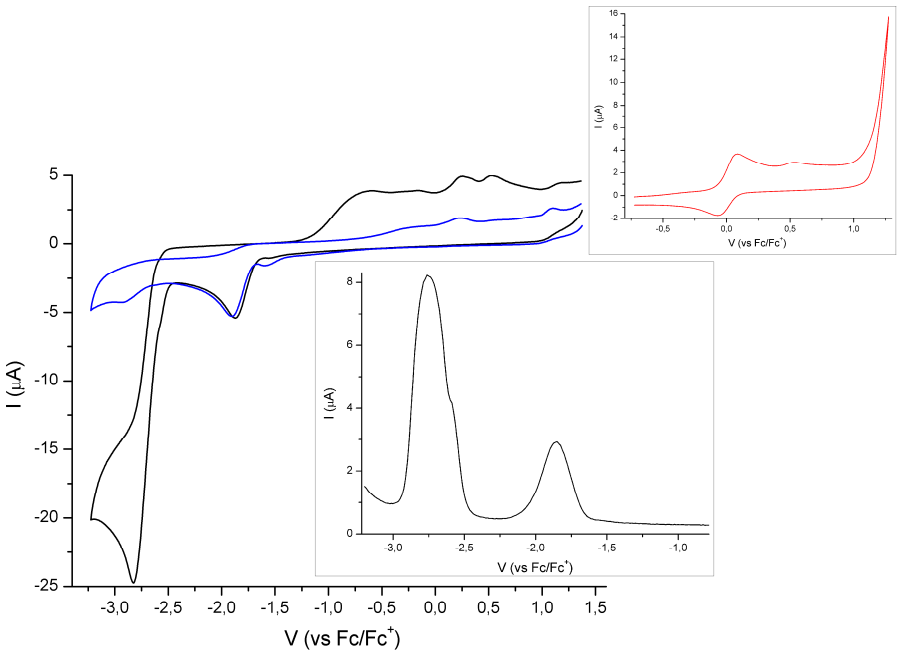

Figure 27. Black line, cyclic voltammetry of btz^{Me} in sulfolane. Glassy carbon electrode, $[NBu_4][PF_6]$ as supporting electrolyte. Blue line, cyclic voltammetry of sulfolane/0.04 M $[NBu_4][PF_6]$. Red line: cyclic voltammetry of ferrocene used as internal reference under the same experimental conditions. Inset: square wave voltammetry of btz^{Me} under the same experimental conditions.

Such a hypothesis is confirmed by DFT calculations on the free ligands. The LUMOs of btz^{Me} and ind^{Me} are qualitatively comparable π^* molecular orbitals, but that of the last compound is about 0.3 eV higher in energy, in agreement with the experimental outcomes.

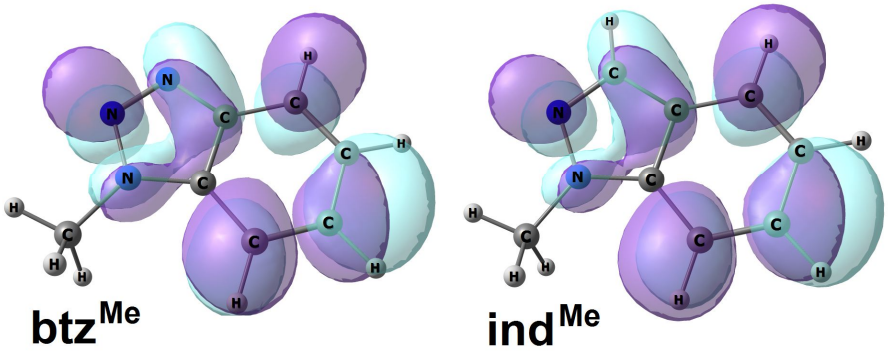

Figure 28. LUMOs of btz^{Me} and ind^{Me} (surface isovalue = 0.03 a.u.).

The studies were subsequently extended with the preparation of bidentate ligands based on the benzotriazole and indazole heterocycles. The 1,1'-bis(azolyl)phenylmethane ligands $CHPh(btz)_2$ and $CHPh(ind)_2$ were obtained by reacting the corresponding 1,1'-carbonylbis-azole derivatives with benzaldehyde in

the presence of catalytic $CoCl_2$. The precursors were obtained following a different method with respect to the one reported in literature, using triphosgene as reactant. The $CoCl_2$-catalyzed approach was then extended to pyridine-2-carboxaldeyde, allowing the isolation of the tridentate ligand 1,1'-bis(benzotriazolyl)-pyridinyl-2-yl-methane $CHPy(btz)_2$, that to the best of our knowledge has never been reported in the literature. Characterization data of this species agree with the proposed formula, and crystals suitable for X-ray diffraction were collected. The structure is depicted in Figure 28. During the purification steps of the other ligands also crystals of 1,1'-bis(benzotriazolyl)phenylmethane were collected, and its structure derived from X-ray diffraction is shown in Figure 28.

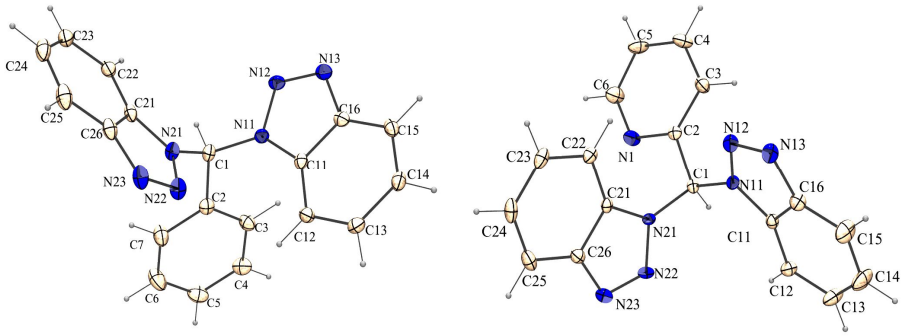

Figure 28. Crystal structures of 1,1'-bis(benzotriazolyl)phenylmethane $CHPh(btz)_2$ and 1,1'-bis(benzotriazolyl)-pyridinyl-2-yl-methane $CHPy(btz)_2$.

The conjugate acid of the ligand $CHPh(btz)_2$ was reacted with the $[Cu(BH_4)(P\text{-}P)]$ precursors following the synthetic approach above described. Characterization data agree with products having general formula $[Cu\{CHPh(btz)_2\}(P\text{-}P)][BF_4]$. In particular, the compounds behave as 1:1 electrolytes in acetone solution. IR spectra indicate the disappearance of borohydride and show vibrations attributable to the N- and P-donor ligands, besides the counter-anion. The presence of $CHPh(btz)_2$ is highlighted in the ^1H NMR spectra by a high frequency shift between 9.10 and 9.20 ppm. ^{31}P $\{^1H\}$ NMR spectra are characterized by a single broad resonance, that can be detected only lowering the temperature in the case of the dppe derivative. As an example, Figure 29 reports the ^1H and ^{31}P $\{^1H\}$ NMR spectra of $[Cu\{CHPh(btz)_2\}(PPh_3)_2][BF_4]$.

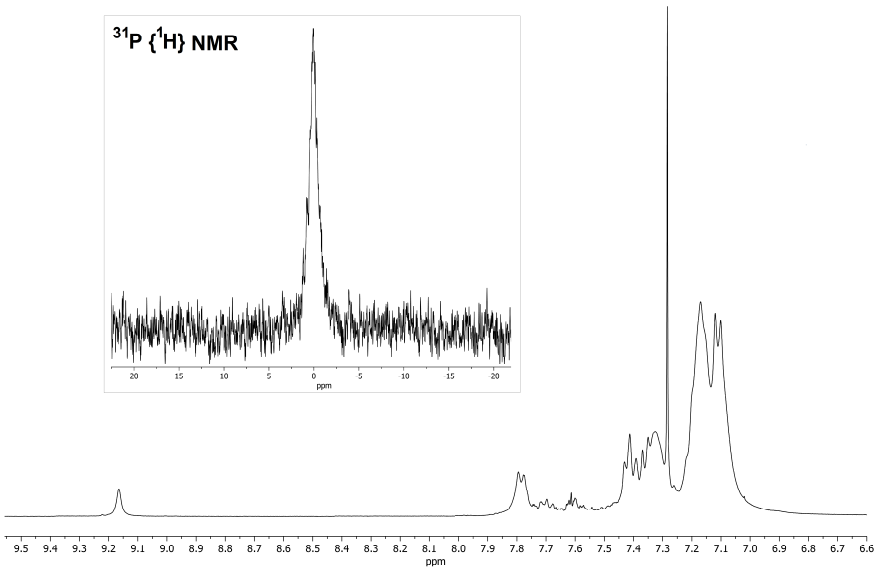

Figure 29. ^{1}H NMR and ^{31}P $\{^{1}H\}$ NMR of $[Cu\{CHPh(btz)_2\}(PPh_3)_2][BF_4]$ ($CDCl_3$, 298 K).

The same methodology was extended to the ligands $CHPh(ind)_2$ and $CHPy(btz)_2$ that, after protonation, were subsequently reacted with $[Cu(BH_4)(PPh_3)_2]$. Characterization data for the $CHPh(ind)_2$ derivative are comparable with those previously described for $[Cu\{CHPh(btz)_2\}(PPh_3)_2][BF_4]$. The presence of the N-donor chelating ligand is confirmed, besides the typical high frequency CH resonance, by a singlet at 7.95 ppm related to the five-membered heterocycles. The presence of only one resonance indicates that the two donor moieties are equivalent on the NMR timescale. The proposed formula is $[Cu\{CHPh(ind)_2\}(PPh_3)_2][BF_4]$.

Thanks to the presence of the pyridine fragment, $CHPy(btz)_2$ can act as tridentate ligand. The displacement of one of the two triphenylphosphine ligands is confirmed by the collected characterization data and the proposed formula is therefore $[Cu\{CHPy(btz)_2\}(PPh_3)][BF_4]$. In particular, the ^{1}H NMR spectrum of the product of the reaction in $CDCl_3$ shows very broad resonances related to the pyridine moiety, that are partially resolved on rising the temperature (see Figure 30). On the contrary, sharp multiplets are present in the ^{1}H NMR spectrum of the species dissolved in the coordinating solvent DMSO-d_6. It is likely to suppose that pyridine is coordinated to Cu(I) and it is displaced by DMSO. The compound maintains fluxional behaviour in both the solvents, as highlighted by the ^{31}P $\{^{1}H\}$ NMR spectra (Figure 30). The reactions between $[Cu(BH_4)(P\text{-}P)]$ precursors and polydentate ligands are summarized in Scheme 11 for clarity.

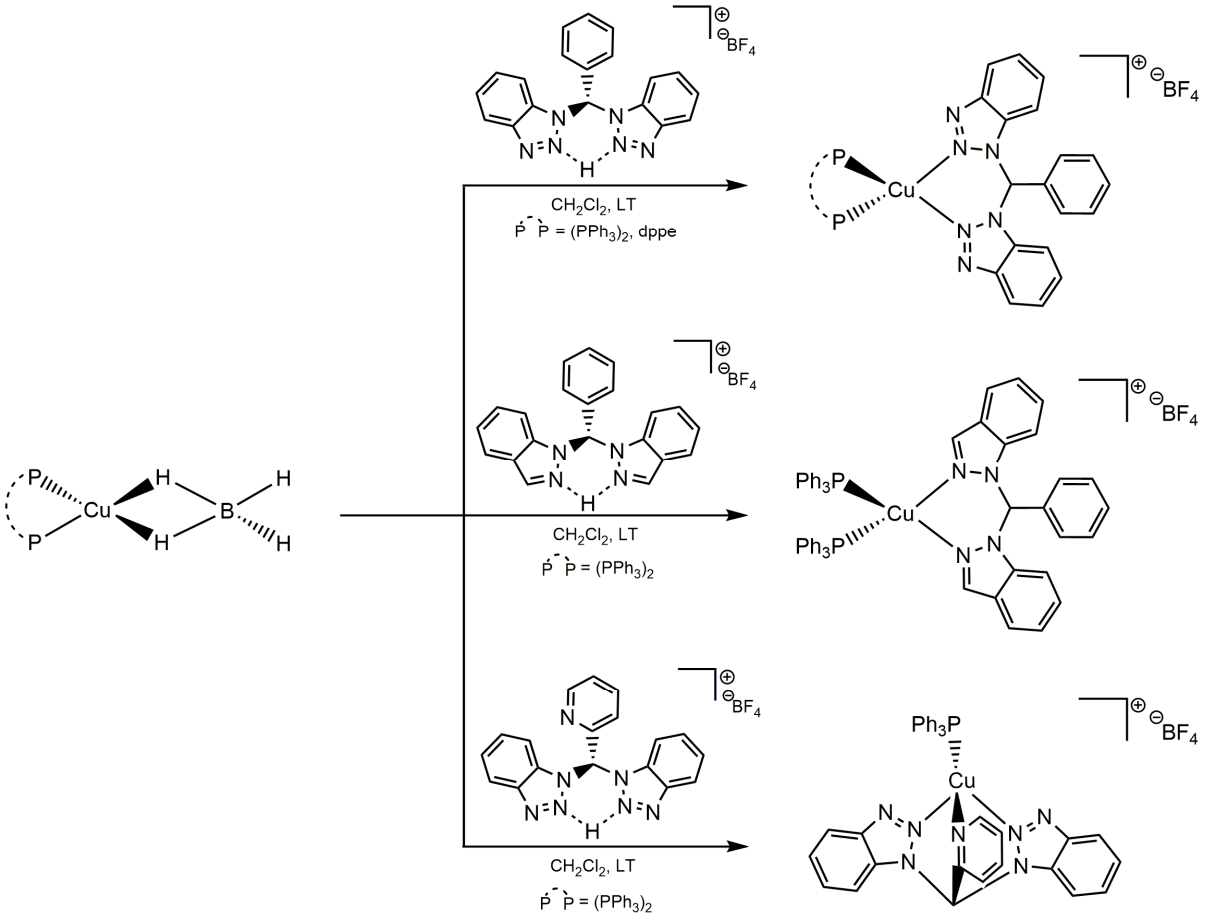

Scheme 11. Synthesis of [Cu{CHPh(btz)$_2$}(P-P)][BF$_4$] [P-P = (PPh$_3$)$_2$ or dppe], [Cu{CHPh(ind)$_2$}(PPh$_3$)$_2$][BF$_4$] and [Cu{CHPy(btz)$_2$}(PPh$_3$)][BF$_4$]

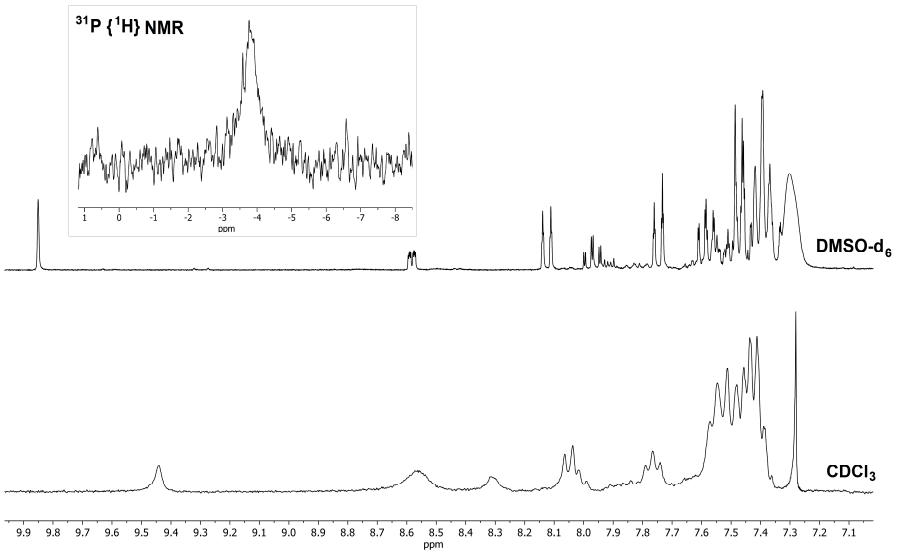

Figure 30. ^{1}H NMR spectra of [Cu{CHPy(btz)$_2$}(PPh$_3$)][BF$_4$] in CDCl$_3$ at 323 K and in DMSO-d$_6$ at 298 K. Inset: ^{31}P {^{1}H} NMR spectrum in DMSO-d$_6$ at 298 K.

Photoluminescence data are in line with the results previously reported for btz^{Me} and ind^{Me} derivatives. [Cu{CHPh(btz)$_2$}(P-P)] complexes are characterized by a noticeable luminescence in the yellow range by excitation with near-UV radiation. The replacement of triphenylphosphine ligands with dppe caused only a lowering of the intensity in the emission band. The ground-state vibrational structure can be detected in the PL spectra and it is comparable with the previous outcomes for other btz-based luminescent species. Lifetime values are in line with the data reported for the btz^{Me} complexes. As an example, Figure 31 reports the PL and PLE spectra of [Cu{CHPh(btz)$_2$}(PPh$_3$)$_2$][BF$_4$]. The formal replacement of the benzotriazole rings with indazole caused a meaningful decrease in the intensity of the emission and a shift of the maximum towards shorter wavelengths, in agreement with the results previously described for ind^{Me} complexes.

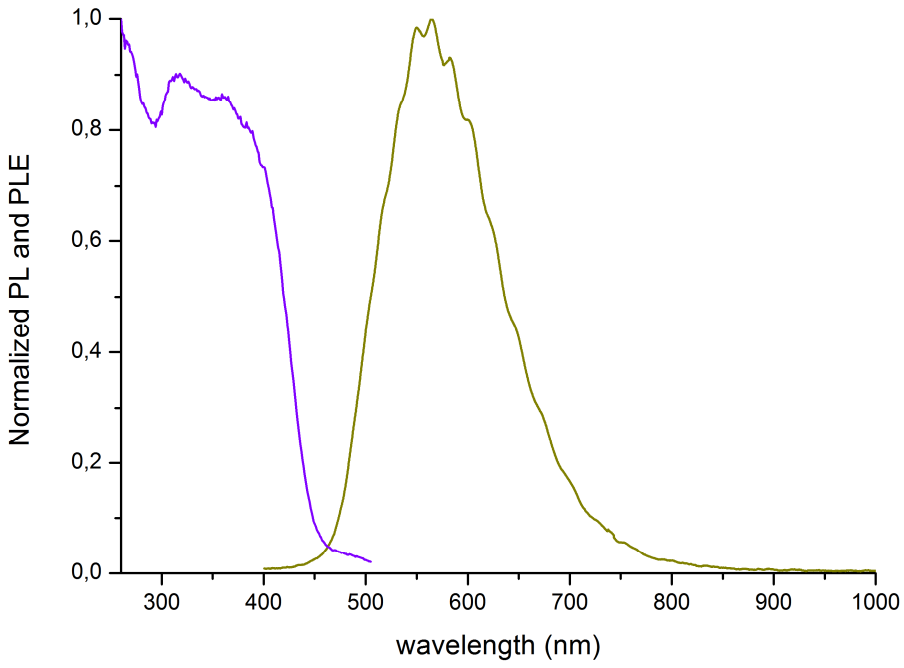

Figure 31. Normalized PL ($\lambda_{excitation}$ = 375 nm, dark yellow line) and PLE ($\lambda_{emission}$ = 586 nm, violet line) spectra of [Cu{CHPh(btz)$_2$}(PPh$_3$)$_2$][BF$_4$]. Solid samples, r.t.

It is noteworthy that coating blue LEDs with yellow-emitting species is a common technological method for the fabrication of white light emitting diodes (WLEDs). Nowadays the most common approach is the encapsulation of indium gallium nitride (InGaN) LEDs with cerium-doped yttrium aluminium garnets (YAG:Ce^{3+}) [48]. The PL and PLE spectra of [Cu{CHPh(btz)$_2$}(PPh$_3$)$_2$][BF$_4$] suggested to be a possible

candidate for such an application. The complex revealed to be stable once embedded in poly(methyl methacrylate) (PMMA) matrix. In a typical preparation, about 2 mg of the complex were dissolved in CH_2Cl_2 (0.5 mL) containing 50 mg of PMMA. The solution thus obtained was used for the coating of UV led with emission maximum at 385 nm, available from the distributor at 0.45 €/piece. The emission spectrum of the coated LED is reported in Figure 32, together with the CIE 1931 chromaticity coordinates (x = 0.354, y = 0.381). The white emission thus obtained has colour temperature of 4800 K, calculated accordingly to McCamy's formula [49], but differences in the balancing of blue and yellow can be obtained by changing the thickness of the coating.

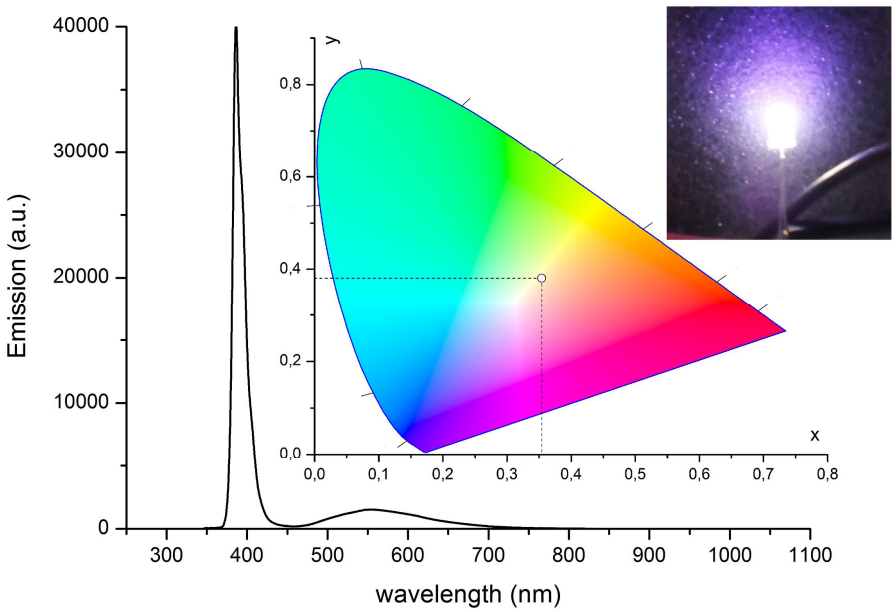

Figure 32. Emission spectrum of a $[Cu\{CHPh(btz)_2\}(PPh_3)_2][BF_4]$ - coated UV led and CIE 1931 chromaticity diagram.

DFT calculations on ground-state singlet $[Cu\{CHPh(btz)_2\}(PPh_3)_2]^+$ suggest that the absorption of radiation is related to the charge transfer from metal- and phosphine-centred orbitals, in particular the HOMO, and unoccupied π^* orbitals of the benzotriazole fragments, such as the LUMO. The frontier orbitals are depicted in Figure 33. The spin density of the DFT-optimized triplet-state geometry shows that the unpaired electrons are localized on the metal centre, the phosphorous atoms and the benzotriazole ring. TD-DFT calculations indicate that the phosphorescence emission involves the previously described molecular orbitals (see Figure 33) and the

computed value is 563 nm, in agreement with the experimental outcomes. It is therefore reasonable to conclude that the emission from $[Cu\{CHPh(btz)_2\}(PPh_3)_2]^+$ has ^{3}MLCT nature.

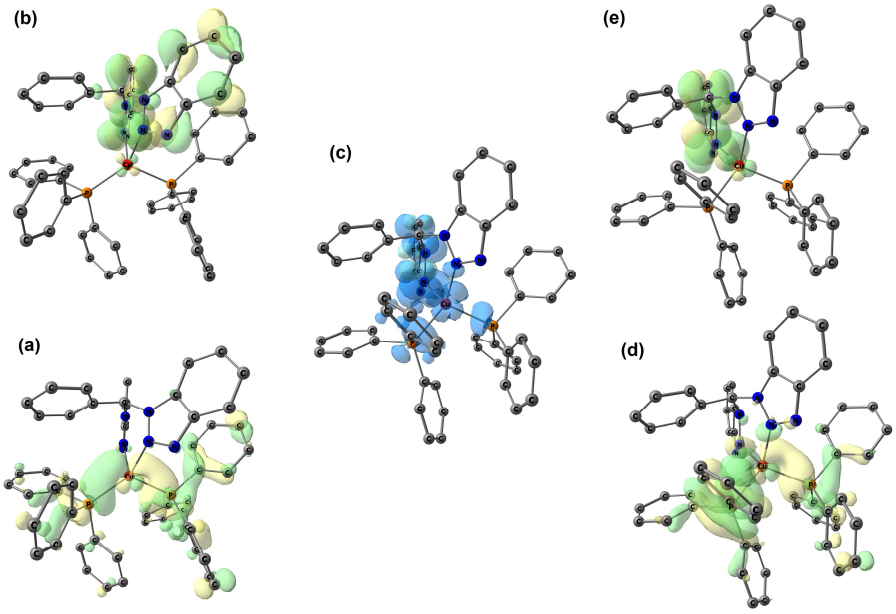

Figure 33. HOMO (a) and LUMO (b) of ground-state singlet $[Cu\{CHPh(btz)_2\}(PPh_3)_2]^+$; triplet-state geometry of $[Cu\{CHPh(btz)_2\}(PPh_3)_2]^+$ with spin density (c) and orbitals involved in the phosphorescent emission (d,e). Surface isovalues: 0.03 a.u. MOs, 0.003 a.u. spin density. Hydrogen atoms are omitted for clarity.

DFT calculations allow to explain the different luminescence of the analogous indazole derivative. As observable in Figure 34, the ground-state frontier orbitals of $[Cu\{CHPh(ind)_2\}(PPh_3)_2]^+$ are qualitatively comparable with those reported in Figure 33, but the energy gap is larger by about 0.5 eV mainly because the LUMO is at higher energy. As explained before, this indicates a more difficult energy transfer, or consequently that the MLCT states are at higher energy with respect to $[Cu\{CHPh(btz)_2\}(PPh_3)_2]^+$. The spin density of the optimized triplet geometry of $[Cu\{CHPh(ind)_2\}(PPh_3)_2]^+$, depicted Figure 34, shows that in this case the lowest excited triplet-state is no more related to the metal-to-ligand charge transfer, but it is instead ligand-centred. The markedly different photoluminescent behaviour is therefore attributable to the strong variation of the relative stability of the excited states, caused by small charges in the heterocycle skeleton.

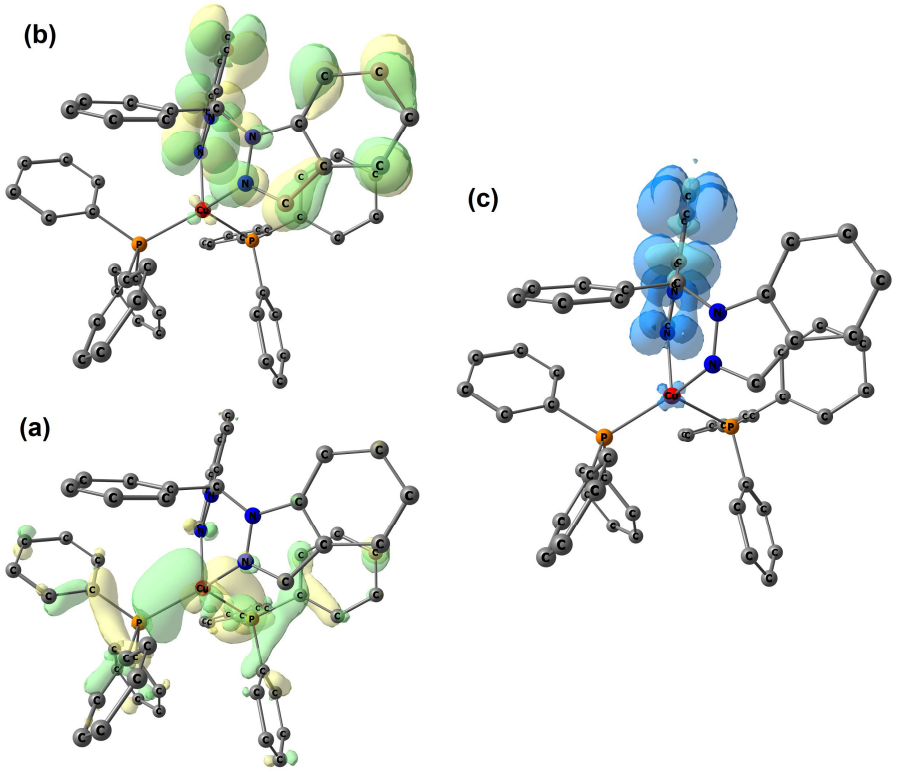

Figure 34. HOMO (a) and LUMO (b) of ground-state singlet $[Cu\{CHPh(ind)_2\}(PPh_3)_2]^+$; triplet-state geometry of $[Cu\{CHPh(ind)_2\}(PPh_3)_2]^+$ with spin density (c). Surface isovalues: 0.03 a.u. MOs, 0.003 a.u. spin density. Hydrogen atoms are omitted for clarity.

The luminescence of the complex $[Cu\{CHPy(btz)_2\}(PPh_3)][BF_4]$ is markedly lower than that of $[Cu\{CHPh(btz)_2\}(PPh_3)_2][BF_4]$, despite the fact that the maxima of the two emissions are very close and the absorption spectra in solution are quite similar. The reduction of luminescence can be related to different factors, such as the lack of one phosphine ligand that, as shown before, participates to the frontier occupied orbital. Another possibility is the involvement of pyridine molecular orbitals in the charge transfer from the metal centre, with the formation of excited states that follow non-radiative decay routes.

The polydentate ligands previously described were reacted also with the acetonitrile precursor $[Cu(NCCH_3)_4][BF_4]$ without the addition of other ancillary ligands, with the aim to isolate homoleptic compounds. In the case of bidentate ligands the characterization data agree with the formation of the complexes $[Cu\{CHPh(btz)_2\}_2][BF_4]$ and $[Cu\{CHPh(ind)_2\}_2][BF_4]$ (Scheme 12).

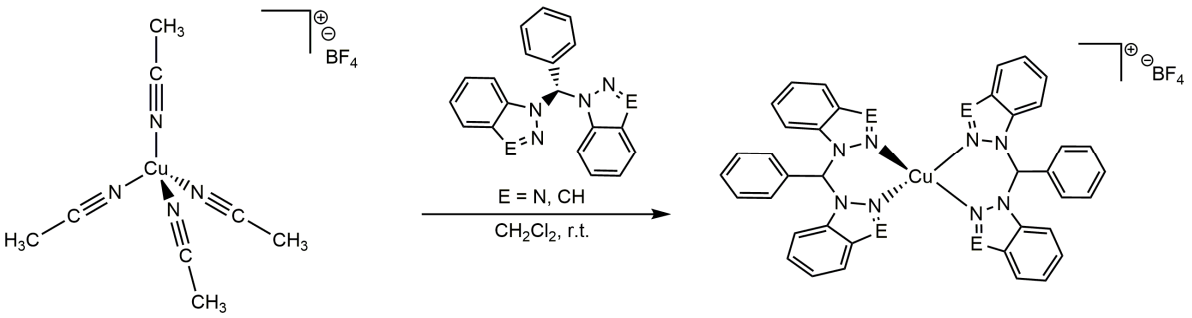

Scheme 12. Synthesis of $[Cu\{CHPh(btz)_2\}_2][BF_4]$ and $[Cu\{CHPh(ind)_2\}_2][BF_4]$

Both the compounds are scarcely soluble in dichloromethane and chloroform. The ^1H NMR spectra in DMSO-d_6 at 298 K show a set of sharp resonances for the benzotriazole derivative, while the signals of $[Cu\{CHPh(ind)_2\}_2][BF_4]$ are broad at 298 K and can be resolved only increasing the temperature (see Figure 35). These data suggest possible fluxional behaviour related to the reversible exchange of the donor moieties with DMSO in the copper coordination sphere. The different σ-donor ability of the two heterocycles, in particular the higher nucleophilicity of indazole [50], can explain the NMR outcomes.

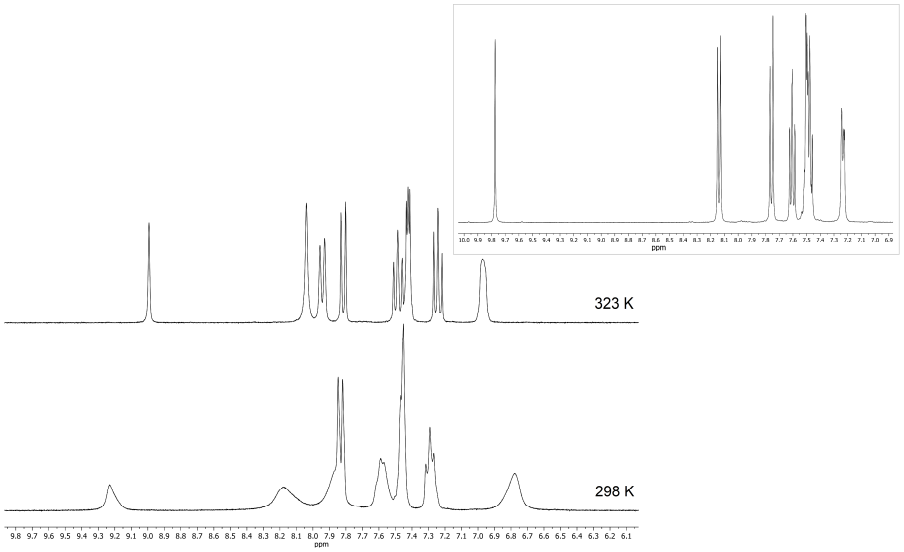

Figure 35. ^1H NMR spectra of $[Cu\{CHPh(ind)_2\}_2][BF_4]$ in DMSO-d_6 at variable temperature. Inset: ^1H NMR of $[Cu\{CHPh(btz)_2\}_2][BF_4]$ in DMSO-d_6 at 298 K.

The formation of homoleptic complexes was indirectly confirmed by the crystals collected from the reaction between CuCl and $CHPh(ind)_2$. X-ray diffraction revealed

that the compound has formula $[Cu\{CHPh(ind)_2\}_2]Cl$, and the structure of the cation is depicted in Figure 36.

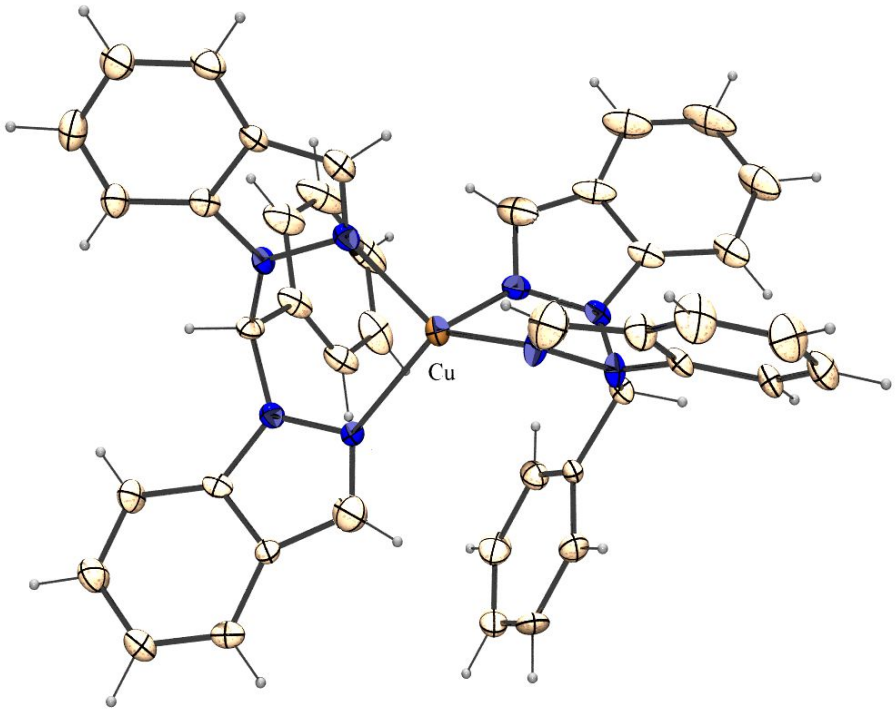

Figure 36. Crystal structure of the cation $[Cu\{CHPh(ind)_2\}_2]^+$.

For what concerns the 1:1 reaction between $[Cu(NCCH_3)_4][BF_4]$ and $CHPy(btz)_2$, the compound that was isolated is not soluble in organic solvents such as dichloromethane and acetone. The ^1H NMR spectrum in DMSO-d_6 is composed by the typical resonances of the ligand and there is no signal attributable to acetonitrile. The lack of coordinated CH_3CN is confirmed by the absence of $\nu_{C\equiv N}$ stretchings in the IR spectrum [51]. For this reason, it is likely to suppose that the complex is polynuclear, with benzotriazole moieties acting as bridging ligands.

The PL spectra of $[Cu\{CHPh(btz)_2\}_2][BF_4]$ and $[Cu\{CHPh(ind)_2\}_2][BF_4]$ are reported in Figure 37. Both the species have emission in the yellow region, but that of the indazole derivative is relatively less intense and blue-shifted. The excitation range of $[Cu\{CHPh(ind)_2\}_2][BF_4]$ is less wide than that of the analogous benzotriazole complex, in agreement with an ipsochromic shift related to the higher LUMO relative energy of indazole with respect to benzotriazole. The luminescence lifetimes are in both the cases of the order of tenths of μs, indicating the involvement of excited states having triplet multiplicity. In the case of $[Cu\{CHPy(btz)_2\}][BF_4]$ the emission

features are quite poor, in agreement with the data previous discussed concerning [Cu{CHPh(btz)$_2$}(PPh$_3$)][BF$_4$].

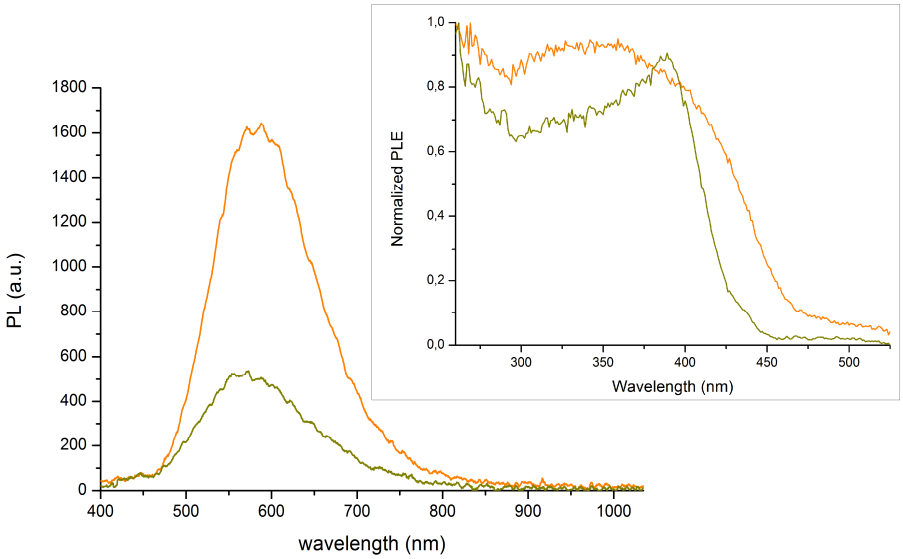

Figure 37. PL spectra of [Cu{CHPh(btz)$_2$}$_2$][BF$_4$] (orange line) and [Cu{CHPh(ind)$_2$}$_2$][BF$_4$] (dark yellow line) under the same experimental conditions (solid samples, r.t., $\lambda_{excitation}$ = 375 nm). Inset: normalized PLE spectra.

During the last part of the thesis CuBr was considered as potential precursor for the preparation of luminescent complexes, using the polydentate ligands previously described. In the case of the indazole-based species the characterization data suggest that the product does not contain coordinated bromide, but the formation of the already described [Cu{CHPh(ind)$_2$}$_2$]$^+$ cation (Figure 36) is instead supported. On the other hand, new products were isolated using the benzotriazole-based ligands, probably because the lower nucleophilicity of the heterocycle makes the displacement of bromide more difficult. The proposed formulae are [CuBr{CHPh(btz)$_2$}]$_x$ and [CuBr{CHPy(btz)$_2$}], but the lack of solubility in non-coordinating solvents prevented an unambiguous characterization of the complexes. In particular, DMSO solutions of the products are conductive, but this can be probably attributed to the displacement of bromide by a solvent molecule. The ^{1}H NMR spectra in DMSO-d$_6$ show only sharp resonances due to the ligands. It is likely to suppose the formation of polynuclear species, in particular for the [CuBr{CHPh(btz)$_2$}]$_x$ derivative, but the experimental data are not sufficient at this moment to define the structure. The emissions of the species are characterized by

quite low intensity and fall in the same range of the previously described benzotriazole-based compounds.

The coordination ability of the tridentate N-donor ligand $CHPy(btz)_2$ and the negative effect on luminescence of the pyridine heterocycle suggested the preparation of a [N,N,N]-donor ligand having similar skeleton, but with another benzotriazole ring replacing the pyridine moiety. Tris(benzotriazolyl)methane, $CH(btz)_3$, was synthesized accordingly to literature methods and preliminarily reacted with CuBr. The product that separates from dichloromethane has bright orange luminescence by excitation with near-UV light. PL and PLE spectra are reported in Figure 38. The measured lifetime is 19 μs, in line with a phosphorescent emission. The NMR data in DMSO-d_6 confirm the coordination of $CH(btz)_3$, but further information is required to define the structure of the complex. The preliminary results here reported however indicate that $CH(btz)_3$ is a promising ligand for copper-based luminescent compounds. It is worth noting that the reported method for the preparation of $CH(btz)_3$ has quite low yield, therefore the development of different synthetic strategies is highly desirable. Benzotriazole can be easily converted in N-formyl-benzotriazole using formic acid and diisopropylcarbodiimide [52]. A possible method to be developed can be based on the $CoCl_2$-catalyzed reaction applied during the thesis, using N-formyl-benzotriazole and 1,1'-carbonylbis(benzotriazole).

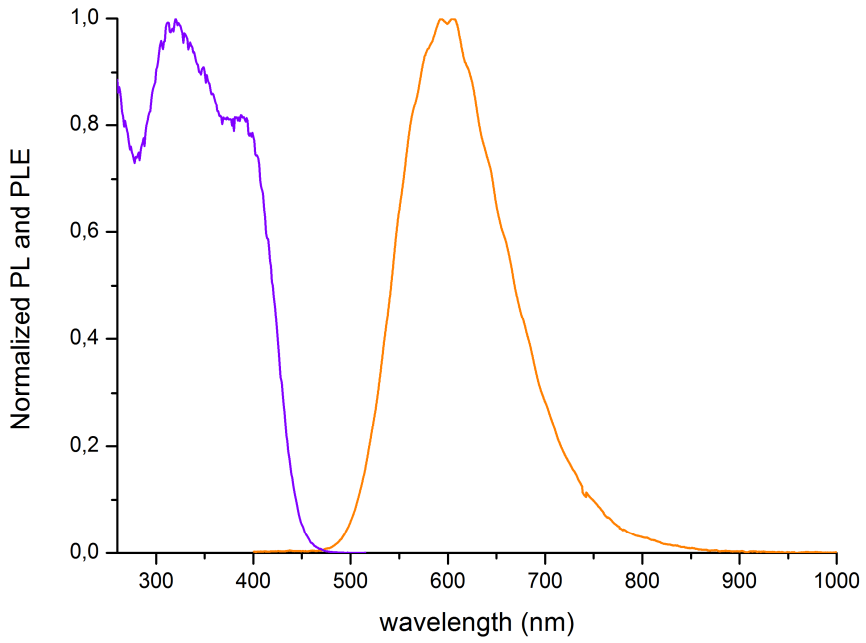

Figure 38. Normalized PL ($\lambda_{excitation}$ = 375 nm, orange line) and PLE ($\lambda_{emission}$ = 614 nm, violet line) spectra of [CuBr{$CH(btz)_3$}]. Solid samples, r.t.

4. Conclusions

During the master's degree internship luminescent copper(I) complexes based on benzotriazole and indazole derivatives were prepared. Most of them exhibited yellow-orange emission after being excited with near-UV light. Microsecond-long lifetimes are in line with triplet-state emissions.

As concerns monodentate ligands, the replacement of btz^{Me} with ind^{Me} in heteroleptic complexes caused a blue-shift of the emission, explained on the basis of voltammetric measurements and DFT calculations on the free heterocycles. The higher LUMO energy of ind^{Me} is at the basis of the different photoluminescent behaviour of its derivatives. The decrease in the intensity of the emission by replacing PPh_3 with dppe in the coordination sphere proved the non-innocent role of the ancillary ligands, the steric bulk in particular.

As regards the polydentate ligands, the photophysical characterization of $CHPh(btz)_2$ and $CHPh(ind)_2$ complexes confirmed the results obtained with related monodentate ligands. The variations in the electronic structure of the heterocycles is at the basis of different photoluminescence mechanisms in heteroleptic compounds, ^{3}MLCT for $[Cu\{CHPh(btz)_2\}(PPh_3)_2]^+$ and ^{3}LC for $[Cu\{CHPh(ind)_2\}(PPh_3)_2]^+$, as indicated by DFT calculations. The noticeable luminescence and good stability of $[Cu\{CHPh(btz)_2\}(PPh_3)_2]^+$ allowed its use for the preparation of yellow-emitting polymeric coatings, potentially interesting in LED technology.

Another difference between benzotriazole- and indazole-based ligands that emerged from the experimental work is the higher nucleophilicity of the latter, causing for instance the displacement of chloride and bromide from the coordination sphere of Cu(I). The homoleptic $[Cu\{CHPh(ind)_2\}]^+$ complex was isolated starting from the precursors CuCl, CuBr and $[Cu(NCCH_3)_4]^+$ and its structure was ascertained by means of X-ray diffraction.

The new tridentate ligand $CHPy(btz)_2$ was synthesized by changing the aldehyde in the $CoCl_2$-catalyzed reactions used for the preparation of the bidentate ligands. The structure was confirmed by X-ray diffraction. Cu(I) complexes with such a species in the coordination sphere resulted however characterized by quite low luminescence. On the other hand, preliminary outcomes indicate the tridentate ligand $CH(btz)_3$ as a promising candidate for the preparation of new Cu(I) luminescent derivatives. Further

studies are required to find new synthetic approaches for the preparation of $CH(btz)_3$ in higher yield.

5. Bibliography

[1] (a) M. Gaft, R. Reisfeld, G. Panczer, *Modern Luminescence Spectroscopy of Minerals and Materials*, 2nd ed., Springer, Heidelberg, 2015. (b) A. Harriman, *Coord. Chem. Rev.* **28** (1979) 147.

[2] V. Balzani, S. Campagna, *Topics in Current Chemistry*, **280**, Springer-Verlag, Berlin, 2007.

[3] Jean-Claude G. Bünzli, *Chem. Rev.* **110** (2010) 2729.

[4] V. Balzani, S. Campagna, *Topics in Current Chemistry*, **281**, Springer-Verlag, Berlin, 2007.

[5] (a) L. Pereira, *Organic Light-Emitting Diodes. The Use of Rare-Earth and Transition Metals*, CRC Press, Boca Raton, 2012. (b) H. Xu, R. Chen, Q. Sun, W. Lai, Q. Su, W. Huang, X. Lu, *Chem. Soc. Rev.* **43** (2014). 3259. (c) V. W.-W. Yam, K. M.-C. Wong, *Chem. Commun.* **47** (2011) 11579.

[6] (a) Y. Yue, T. Grusenmeyer, Z. Ma, P. Zhang, R. H. Schmehl, D. N. Beratan, I. V. Rubtsov, *J. Phys. Chem. A* **118** (2014) 10407. (b) V.W.W. Yam and K.K.W. Lo, *Chem. Soc. Rev.* **28** (1999) 323.

[7] P. Atkins, J. De Paola, *Physical Chemistry,* 8th ed., OUP Oxford, 2006.

[8] (a) P. Chen, T. J. Meyer, *Chem. Rev.* **98** (1998) 1439. (b) A. Juris, V. Balzani, F. Barigelletti, S. Campagna, P. Belser, A. von Zelewsky, *Coor. Chem. Rev.* **84** (1988) 85. (c) K. Kalyanasundaram, *Coor. Chem. Rev.* **46** (1982) 159.

[9] Q. C. Zhang, H. Xiao, X. Zhang, L. J. Xu, Z. N. Chen, *Coor. Chem. Rev.* **378** (2019) 121.

[10] (a) L. A. Büldt, O. S. Wenger, *Chem. Sci.* **8** (2017) 7359. (b) P. Chábera, Y. Liu, O. Prakash, E. Thyrhaug, A. El Nahhas, A. Honarfar, S. Essén, L.A. Fredin, T.C.B. Harlang, K.S. Kjær, K. Handrup, F. Ericson, H. Tatsuno, K. Morgan, J. Schnadt, L. Häggström, T. Ericsson, A. Sobkowiak, S. Lidin, P. Huang, S. Styring, J. Uhlig, J. Bendix, R. Lomoth, V. Sundström, P. Persson, K. Wärnmark, *Nature* **543** (2017) 695. (c) J. Chen, Q. Zhang, F. K. Zheng, Z. F. Liu, S. H. Wang, A. Q. Wua, G. C. Guoa

Dalton Trans. **44** (2015) 3289. (d) D. Hausmann, A. Kuzmanoski, C. Feldmann, *Dalton Trans.* **45** (2016) 6541.

[11] Y. Liu, S. C. Yiu, C. L. Ho, W. Y. Wonga, *Coor. Chem. Rev.* **375** (2018) 514.

[12] (a) A. Vogler, H. Kunkely, *J. Am. Chem. Soc.* **108** (1986) 7211. (b) K. R. Kyle, P. C. Ford, *J. Am. Chem. Soc.* **111** (1989) 5005. (c) K. R. Kyle, C. K. Ryu, P. C. Ford, J. A. Di Benedetto, *J. Am. Chem. Soc.* **113** (1991) 2954. (d) A. Dossing, C. K. Ryu, S. Kudo, P. C. Ford, *J. Am. Chem. Soc.* **115** (1993) 5132. (e) F. De Angelis, S. Fantacci, A. Sgamellotti, E. Cariati, R. Ugo, P. C. Ford, *Inorg. Chem.* **45** (2006) 10576. (f) P. C. Ford, E. Cariati, J. Bourassa, *Chem. Rev.* **99** (1999) 3625.

[13] (a) Y. Tao, K. Yuan, T. Chen, P. Xu, H. Li, R. Chen, C. Zheng, L. Zhang, W. Huang, *Adv. Mater.* **26** (2014) 7931. (b) G. Lia, Z. Q. Zhu, Q. Chen, J. Li, *Organic Electronics* **69** (2019) 135. (c) R. Czerwieniec, J. Yu, H. Yersin, *Inorg. Chem.* **50** (2011) 8293. (d) M. J. Leitl, F. R. Küchle, H. A. Mayer, L. Wesemann, H. Yersin, *J. Phys. Chem. A* **117** (2013) 11823.

[14] (a) C. Bizzarri, C. Fléchon, O. Fenwick, F. Cacialli, F. Polo, M. D. Gálvez-López, C. H. Yang, S. Scintilla, Y. Sun, R. Fröhlich, L. De Cola, *ECS J. Solid State Sci. Technol.* **5** (2016) R83. (b) M. Ruthkosky, C. A. Kelly, F. N. Castellano, G. J. Meyer, *Coor. Chem. Rev.* **171** (1998) 309.

[15] D. V. Scaltrito, D. W. Thompson, J. A. O'Callaghan, G. J. Meyer, *Coor. Chem. Rev.* **208** (2000) 243.

[16] (a) R. A. Rader, D. R. McMillin, M. T. Buckner, T. G. Matthews, D. J. Casadonte, R. K. Lengel, S. B. Whittaker, L. M. Darmon, F. E. Lytle, *J. Am. Chem. Soc*. **103** (1981) 5906. (b) K. Kubiček, S.T. Veedu, D. Storozhuk, R. Kia, S. Techert, *Polyhedron* **124** (2017) 166. (c) C. Bizzarri, C. Strabler, J. Prock, B. Trettenbrein, M. Ruggenthaler, C. H. Yang, F. Polo, A. Iordache, P. Brüggeller, L. De Cola, *Inorg. Chem.* **53** (2014) 10944.

[17] A. R. Cabrera, I. A. Gonzalez, D. Cortés-Arriagada, M. Natali, H. Berke, C. G. Daniliuc, M. B. Camarada, A. Toro-Labbé, R. S. Rojas, C. O. Salas, *RSC Adv.* **6** (2016) 5141.

[18] Q. Zhang, Q. Zhou, Y. Cheng, L. Wang, D. Ma, X. Jing, F. Wang, *Adv. Mater.* **16** (2004) 423.

[19] Q. Zhang, J. Ding, Y. Cheng, L. Wang, Z. Xie, X. Jing, F. Wang, *Adv. Funct. Mater.* 17 (2007) 2983.

[20] F. Parmeggiani, A. Sacchetti, *J. Chem. Educ.* **89** (2012) 946.

[21] E. Cariati, E. Lucenti, C. Botta, U. Giovanella, D. Marinotto, S. Righetto, *Coor. Chem. Rev.* **306** (2016) 566.

[22] (a) F. Liu, Y. Jin, B. Liu, R. Li, Y. Deng, W. Li, F. Jian, *Chin. J. Chem.* **30** (2012) 1069. (b) J. L. Chen, P. Song, J. Liao, H. R. Wen, R. Hong, Z. N. Chen, Y. Chi, *Inor. Chem. Comm.* **13** (2010) 1057. (c) J. L. Chen, Z. H. Guo, H. G. Yu, L. H. He, S. J. Liu, H. R. Wen, J. Y. Wang, *Dalton Trans.* **45** (2016) 696.

[23] L. Bergmann, C. Braun, M. Nieger, S. Bräse, *Dalton Trans.* **47** (2018) 608.

[24] (a) M. D. Allendorf, C. A. Bauer, R. K. Bhakta, R. J. T. Houk, *Chem. Soc. Rev.* **38** (2009) 1330. (b) Y. Bai, G. J. He, Y. G. Zhao, C. Y. Duan, D. B. Dang, Q. J. Meng, *Chem. Commun.* (2006) 1530.

[25] (a) R. Peng, M. Li, D. Li, *Coor. Chem. Rev.* **254** (2010) 1. (b) X. Q. Liang, H. P. Xiao, B. L. Liu, Y. Z. Li, J. L. Zuo, X. Z. You, *Polyhedron* **27** (2008) 2494. (c) J. Troyano, J. Perles, P. Amo-Ochoa, J. I. Martínez, M. Concepción Gimeno, V. Fernández-Moreira, F. Zamora, S. Delgado, *Chem. Eur. J.* **22** (2016) 18027.

[26] L. P. Xue, J. J. Tao, *J. Clust. Sci.* **27** (2016) 1729.

[27] E. Lucenti, E. Cariati, A. Previtali, D. Marinotto, A. Forni, V. Bold, V. Ch. Kravtsov, M. S. Fonari, S. Galli, L. Carlucci, *Cryst. Growth Des.* **19** (2019) 1567.

[28] (a) N. Thejo Kalyania, S.J. Dhobleb, *Ren. Sustain. Energy Rev.* **16** (2012) 2696. (b) H. Yersin, A. F. Rausch, R. Czerwieniec, T. Hofbeck, T. Fischer, *Coor. Chem. Rev.* **255** (2011) 2622.

[29] (a) R. D. Costa, E. Ortí, H. J. Bolink, F. Monti, G. Accorsi, N. Armaroli, *Angew. Chem. Int. Ed.* **51** (2012) 8178.

[30] (a) S. H. Kong, J. I. Lee, S. Kim, M. S. Kang, *ACS Photonics* **5** (2018) 267. (b) B. High, D. Bruce, M. M. Richter, *Anal. Chim. Acta* **449** (2001) 17.

[31] M. Bortoluzzi, J. Castro, M. Girotto, F. Enrichi, A. Vomiero, *Inor. Chem. Comm.* **102** (2019) 141.

[32] W. L. F. Armarego, D. D. Perrin, *Purification of laboratory chemicals*, 4th ed., Butterworth Heinemann, Oxford, 1996.

[33] R. N. Keller, H. D. Wycoff, *Inorg. Synth.* **2** (1946) 1.

[34] W. J. Geary, *Coord. Chem. Rev.* **7** (1971) 81.

[35] (a) I. C. Gerber, J. G. Ángyán, *Chem. Phys. Lett.* **415** (2005) 100. (b) J. D. Chai, M. Head-Gordon, *Phys. Chem. Chem. Phys.* **10** (2008) 6615. (c) Y. Minenkov, Å. Singstad, G. Occhipinti, V. R. Jensen, *Dalton Trans.* **41** (2012) 5526. (d) F. Weigend, R. Ahlrichs, *Phys. Chem. Chem. Phys.* **7** (2005) 3297.

[36] M. J. Frisch, G. W. Trucks, H. B. Schlegel, G. E. Scuseria, M. A. Robb, J. R. Cheeseman, G. Scalmani, V. Barone, B. Mennucci, G. A. Petersson, H. Nakatsuji, M. Caricato, X. Li, H. P. Hratchian, A. F. Izmaylov, J. Bloino, G. Zheng, J. L. Sonnenberg, M. Hada, M. Ehara, K. Toyota, R. Fukuda, J. Hasegawa, M. Ishida, T. Nakajima, Y. Honda, O. Kitao, H. Nakai, T. Vreven, J. A. Montgomery Jr., J. E. Peralta, F. Ogliaro, M. Bearpark, J. J. Heyd, E. Brothers, K. N. Kudin, V. N. Staroverov, R. Kobayashi, J. Normand, K. Raghavachari, A. Rendell, J. C. Burant, S. S. Iyengar, J. Tomasi, M. Cossi, N. Rega, J. M. Millam, M. Klene, J. E. Knox, J. B. Cross, V. Bakken, C. Adamo, J. Jaramillo, R. Gomperts, R. E. Stratmann, O. Yazyev, A. J. Austin, R. Cammi, C. Pomelli, J. W. Ochterski, R. L. Martin, K. Morokuma, V. G. Zakrzewski, G. A. Voth, P. Salvador, J. J. Dannenberg, S. Dapprich, A. D. Daniels, Ö. Farkas, J. B. Foresman, J. V. Ortiz, J. Cioslowski, D. J. Fox, *Gaussian 09, Revision C.01*, *Gaussian, Inc., Wallingford CT, 2009*.

[37] J. N. Taylor, E. Emer, S. Preshlock, M. Schedler, M. Tredwell, S. Verhoog, J. Mercier, C. Genicot, V. Gouverneur, *J. Am. Chem. Soc.* **139** (2017) 8267.

[38] H. J. Liu, S. F. Hung, C. L. Chen, M. H. Lin, *Tetrahedron* **69** (2013) 3907.

[39] (a) A. R. Katritzky, D. P. M. Pleynet, B. Yang, *J. Org. Chem.* **62** (1997) 4155. (b) J. W. Nieuwenhuijzen, P. G. M. Conti, H. C. J. Ottenheijm, J. T. M. Linders, *Tetrahedron Letters* **39** (1998) 7811.

[40] K. v. Auwers, E. Frese, *Chem. Ber.* **58** (1925) 2081.

[41] B. S. Hammes, C. J. Carrano, *Inorg. Chem.* **38** (1999) 3562.

[42] (a) Z. Zhong, R. Hong, X. Wang, *Tetrahedron Lett.* **51** (2010) 6763. (b) P. Ballesteros, J. Elguero, R.M.Claramunt, *Tetrahedron* **41** (1985) 5955.

[43] A. R. Katritzky, Z. Yang, J. N. Lam, *Synthesis* (1990) 666.

[44] C. Bianchini, C. A. Ghilardi, A. Meli, S. Midollini, A. Orlandini, *Inorg. Chem.* **24** (1985) 924.

[45] G. J. Kubas, *Inorg. Synth.* **28** (1990) 68.

[46] (a) T. Wu, M. Li, D. Li, X.C. Huang, *Cryst. Growth Des.* **8** (2008) 568. (b) Q. G. Zhai, Y. N. Zhao, S. N. Li, Y. C. Jiang, M.C. Hu, *Inorg. Chem. Commun.* **35** (2013) 31. (c) X. Gao, Q. G. Zhai, S. N. Li, R. Xia, H. J. Xiang, Y. C. Jiang, M.C. Hu, *J. Solid State Chem.* **183** (2010) 1150. (d) M. C. Hu, Y. Wang, Q. G. Zhai, S. N. Li, Y.C. Jiang, Y. Zhang, *Inorg. Chem.* **48** (2009) 1449.

[47] A. J. Bard, L. R. Faulkner, *Electrochemical methods, 2*nd ed., Wiley, New York, 2001.

[48] (a) A. Kitai, *Luminescent materials and applications*, 1st ed., Wiley, Chichester, 2008. (b) P. P. Zak, V. A. Lapina, T. A. Pavich, A. V. Trofimov, N. N. Trofimova, Y. B. Tsaplev, *Russ. Chem. Rev.* **86** (2017) 831. (c) P. Schlotter, R. Schmidt, J. Schneider, *Appl. Phys. A* **64** (1997) 417.

[49] Z. Ghassemlooy, L. N. Alves, S. Zvánovec, M. A. Khalighi, *Visible light communications: theory and applications,* 1st ed., CRC Press, Boca Raton, 2017.

[50] M. Lõkov, S. Tshepelevitsh, A. Heering, P. G. Plieger, R. Vianello, I. Leito, *Eur. J. Org. Chem.* (2017) 4475.

[51] K. Nakamoto, *Infrared and Raman Spectra of Inorganic and Coordination Compounds,* 6th ed., Wiley, Hoboken, 2008.

[52] J. E. Mathieson, J. J. Crawford, M. Schmidtmann, R. Marquez, *Org. Biomol. Chem.* **7** (2009) 2170.